AD-A116 744 AIR FORCE INST OF TECH WRIGHT-PATTERSON AFB OH F/G 20/6
TRANSVERSE EFFECTS IN OPTICAL BISTABILITY AND SUPERFLUORESCENCE--ETC(U)
1982 E A WATSON
UNCLASSIFIED AFIT/NR-82-5T NL

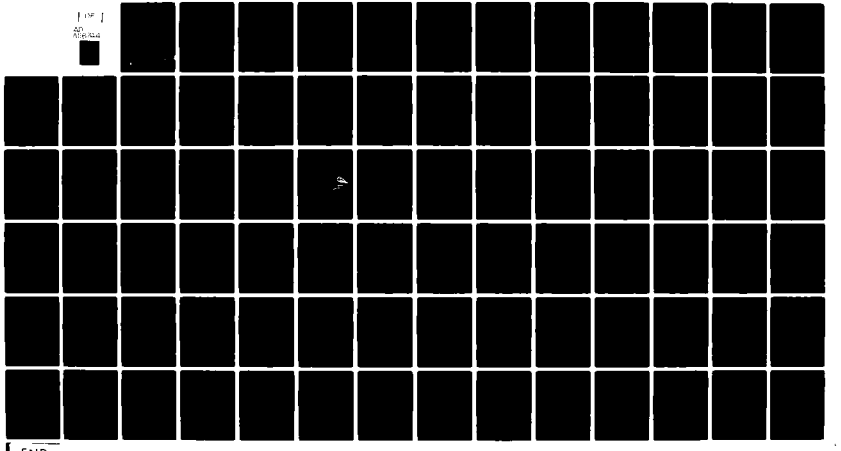

END
DATE FILMED
8-82
DTIC

UNCLASS

SECURITY CLASSIFICATION OF THIS PAGE (When Data Entered)

AD A116744

REPORT DOCUMENTATION PAGE		READ INSTRUCTIONS BEFORE COMPLETING FORM
1. REPORT NUMBER AFIT/NR/82-5T	2. GOVT ACCESSION NO.	3. RECIPIENT'S CATALOG NUMBER
4. TITLE (and Subtitle) Transverse Effects in Optical Bistability and Superfluorescence		5. TYPE OF REPORT & PERIOD COVERED THESIS/DISSERTATION 6. PERFORMING ORG. REPORT NUMBER
7. AUTHOR(s) Edward Alan Watson		8. CONTRACT OR GRANT NUMBER(s)
9. PERFORMING ORGANIZATION NAME AND ADDRESS AFIT STUDENT AT: University of Arizona		10. PROGRAM ELEMENT, PROJECT, TASK AREA & WORK UNIT NUMBERS
11. CONTROLLING OFFICE NAME AND ADDRESS AFIT/NR WPAFB OH 45433		12. REPORT DATE 1982 13. NUMBER OF PAGES 74
14. MONITORING AGENCY NAME & ADDRESS(if different from Controlling Office)		15. SECURITY CLASS. (of this report) UNCLASS 15a. DECLASSIFICATION/DOWNGRADING SCHEDULE

16. DISTRIBUTION STATEMENT (of this Report)

APPROVED FOR PUBLIC RELEASE; DISTRIBUTION UNLIMITED

17. DISTRIBUTION STATEMENT (of the abstract entered in Block 20, if different from Report)

18. SUPPLEMENTARY NOTES

APPROVED FOR PUBLIC RELEASE: IAW AFR 190-17

22 JUN 1982

Lynn Wolaver

LYNN E. WOLAVER
Dean for Research and Professional Development
AIR FORCE INSTITUTE OF TECHNOLOGY (ATC)
WRIGHT-PATTERSON AFB, OH 45433

19. KEY WORDS (Continue on reverse side if necessary and identify by block number)

20. ABSTRACT (Continue on reverse side if necessary and identify by block number)

ATTACHED

82 07 07 066

DTIC FILE COPY

DTIC ELECTE JUL 12 1982 S D E

DD FORM 1 JAN 73 1473 EDITION OF 1 NOV 55 IS OBSOLETE

UNCLASS

SECURITY CLASSIFICATION OF THIS PAGE (When Data Entered)

TRANSVERSE EFFECTS IN OPTICAL BISTABILITY AND SUPERFLUORESCENCE

by

Edward Alan Watson

A Thesis Submitted to the Faculty of the

COMMITTEE ON OPTICAL SCIENCES (GRADUATE)

In Partial Fulfillment of the Requirements
For the Degree of

MASTER OF SCIENCE

In the Graduate College

THE UNIVERSITY OF ARIZONA

1 9 8 1

STATEMENT BY AUTHOR

This thesis has been submitted in partial fulfillment of requirements for an advanced degree at The University of Arizona and is deposited in the University Library to be made available to borrowers under rules of the Library.

Brief quotations from this thesis are allowable without special permission, provided that accurate acknowledgment of source is made. Requests for permission for extended quotation from or reproduction of this manuscript in whole or in part may be granted by the head of the major department or the Dean of the Graduate College when in his judgment the proposed use of the material is in the interests of scholarship. In all other instances, however, permission must be obtained from the author.

SIGNED: _____

APPROVAL BY THESIS DIRECTOR

This thesis has been approved on the date shown below:

_____ _____

HYATT M. GIBBS Date

Professor of Optical Sciences

ACKNOWLEDGMENTS

I would like to gratefully acknowledge the direction, encouragement, and patient tutoring I received from Professor Hyatt Gibbs. I would like to thank Dr. Jerry Moloney and Professor Fred Hopf for many helpful discussions. Additional thanks goes to Dr. Moloney for his assistance in taming an often belligerent computer. Thanks also to K. Tai for his help in performing the experiment.

My deepest appreciation goes to my wife, Cynthia, without whose patience and support I could not have completed this work.

TABLE OF CONTENTS

LIST OF ILLUSTRATIONS

LIST OF ILLUSTRATIONS--Continued

ABSTRACT

The interaction of a light beam with matter has varying degrees of dependence on the transverse profile of the beam. Two topics are considered here. The first topic, superfluorescence, involves the coherent emission generated by an initially inverted two-level medium. Calculations in the past have included either quantum fluctuations in the initial conditions or transverse effects, but never both. The calculations presented here include both transverse effects and quantum fluctuations. The results of the theoretical calculations are in good agreement with previous experimental results, both quantitatively in terms of time delay averages and distributions and also qualitatively in terms of pulse shapes. The second topic considered, optical bistability, involves devices which exhibit two stable output light intensities (a high and a low branch) over a limited range of input light intensities. Simulations performed here show the effect of diffraction, measured in terms of the Fresnel number, on how much of the device becomes bistable. It was found that for small Fresnel number cases, the entire device becomes bistable. For high Fresnel number cases, only part of the device becomes bistable while the rest of the device remains low transmitting. The results of an experiment performed are consistent with the simulations.

CHAPTER 1

INTRODUCTION

The purpose of this thesis is to investigate certain radiation-matter interaction problems in which a transverse dimension is included. Transverse dimensions are spatial directions perpendicular to the direction of propagation of the radiation. When a radiation propagation problem is first investigated, the radiation wavefront is normally assumed to be a uniform plane-wave, i.e., the wavefront has no transverse spatial dependence. This paper presents the results of investigations into the effects of relaxing the uniform plane-wave assumption in two cases of radiation-matter interaction.

The first topic investigated using computer simulations was the effects of including transverse dimensions in superfluorescence. As will be described more fully later, superfluorescence deals with coherent pulse evolution in an initially inverted medium. The pulse is initiated by spontaneous emission, which is modeled statistically. Calculations in the past have been done which included statistics, but did not include transverse dimensions in the problem. Conversely, calculations in the past have been done which included transverse dimensions but did not include statistical modeling of the initiation process. The first part of this paper presents the results of including both statistics and transverse dimensions in the superfluorescence calculation. The relaxing

of the uniform plane-wave assumption and inclusion of statistics are done in an attempt to improve the agreement between theory and experiment.

The second topic investigated using computer simulations and experimentation was in the area of optical bistability. Optical bistability is a relatively new field in which a system with feedback of some sort can output two stable values of light intensity for a single value of the input light intensity. Since this is a relatively new field, there are some basic questions on the physics of the devices which have not been answered. Two of these questions are how far in the transverse direction does the device exhibit bistability, and how does changing the Fresnel number of the system affect the transverse variations. Transverse effects are believed to be important in optical bistability because most of the devices use a laser beam, which has a nonuniform transverse profile, as input.

The two topics just discussed were chosen for this work because of the current interest in the subjects as well as the similarities and differences in the physics involved. Both subjects deal with the interaction of radiation and matter. Both subjects are mathematically modeled by using coupled Maxwell-Bloch equations. Differences between the subjects are that superfluorescence requires an initially inverted (gain) medium, while optical bistability requires some type of nonlinear dispersive or absorptive medium. Bistability also requires some form of optical feedback, while superfluorescence does not. Thus these two topics were investigated for this work because of their interest and the breadth of experience they would supply.

This paper is organized in the following manner: Chapter 2 deals with the superfluorescence calculations, including a description of the physics involved, the modeling and computer program used, and the results and conclusions. Chapter 3 discusses the calculations done in optical bistability, including a description of the physics involved, the model used, and the results and conclusions. The final chapter contains the description and results of an experiment studying transverse effects in optical bistability.

CHAPTER 2

SUPERFLUORESCENCE

Description of Superfluorescence

Superfluorescence (Dicke, 1954; Eberly and Rehler, 1969; Rehler and Eberly, 1971; Bonifacio, Schwendimann and Haake, 1971; Bonifacio and Lugiato, 1975a, 1975b; Skribanowitz et al., 1973; MacGillivray and Feld, 1976, 1981; Degiorgio, 1971) is the name given to the process whereby a pulse of light is emitted from an initially inverted medium which has no initial macroscopic polarization. No input pulse is used to achieve this output pulse. The medium, which consists of two-level atoms, is prepared initially in the upper state. Under semiclassical theory, the medium should remain forever in this inverted state. However, because of spontaneous emission, some of the atoms begin to decay, emitting radiation. These emissions are in all directions. If the medium is made so that it is long and narrow, like a pencil, then the small polarization induced by the spontaneously emitted radiation quantum drives a field which grows significantly in only one dimension. Therefore, once an atom emits radiation such that the induced field travels down the long length of the rod, then it experiences a large gain from the remainder of the inverted system. Hence, superfluorescence is a cooperative, coherent process. It is, in fact, at one of the coherent limits. The radiation fields respond quickly compared to medium response times.

In order for superfluorescence to be a cooperative process, it must occur in a time less than the relaxation times of the medium. The process is characterized by two times, the delay time τ_D, and the superfluorescence time τ_R. The delay time is the time between the inversion of the medium and peak of the output pulse. The superfluorescence time is defined as

$$\tau_R = \frac{8 \pi \tau_o}{3 n \lambda^2 L} \quad , \tag{1}$$

where τ_o = spontaneous lifetime of the inversion, n is the inversion density, λ is the emitted wavelength, and L is the length of the inverted medium. τ_R is roughly the time for a photon to be spontaneously emitted along the length of the sample. Hence the time requirements for superfluorescence are

$$\tau_R < \tau_D < T_1, T_2 \quad , \tag{2}$$

where T_1 and T_2 are medium relaxation times as will be discussed more fully later.

Modeling of Superfluorescence

There are two separate portions to the modeling scheme of superfluorescence used in this investigation. The first is the modeling of the initiation, which involves spontaneous emission and is therefore quantum electrodynamical (QED) in nature. The second part is the evolution and propagation of the pulse along the length of the rod, which is semiclassical.

The initiation, as has been stated, depends upon the spontaneous emission of the atoms initially in the upper state. QED calculations (Haake et al., 1979a; Polder, Schuurmans and Vrehen, 1979; Haake et al., 1980; Haake et al., 1979b) have been done which describe the initiation process. Because of the magnitude of the number of atoms in a typical superfluorescence experiment, it would be extremely difficult to incorporate the QED calculations into a numerical simulation. However, the QED calculations have shown that the QED effects can be modeled statistically in the following manner.

The medium interacts with the pulse radiation through the polarization of the medium generated by the radiation. The polarization is not present until spontaneous emission occurs, since a purely inverted medium does not have a polarization. Once some emission occurs along the pencil, it polarizes the medium; this polarization serves as a source for more emissions which further polarize the medium. This process continues in a self-consistent manner according to the Maxwell-Bloch equations, thereby building the fields in the medium. Because of the statistical nature of the initiation process, the polarizations and fields generated in repeated experiments with the same initial conditions are different. These statistics are reflected in the QED calculations by the statistical properties of the polarization operators. The QED calculations have shown, however, that there is no difference between applying the operators in a purely quantum manner or in disregarding the QED nature of the initiation and assuming that each part of the medium has a small classical initial polarization with a specified variance to account for quantum

fluctuations. In other words, the quantum uncertainties contained in the QED operators which describe the fluctuations of the polarization are replaced by the uncertainties in the classical initial polarizations. The initial polarization of the medium, then, contains all of the quantum fluctuations of the process. The remainder of the superfluorescence process is deterministic and can be handled semiclassically. By averaging over several simulations (or experiments), expectation values of the quantum operators can be reproduced. To describe the statistical initialization of the polarization, the notion of a tipping angle is introduced. The tipping angle can be regarded as the fluctuation in the Bloch vector that is produced by the polarization induced by the spontaneous emission (see Fig. 1). The tipping angle moves the vector off of the w axis (w no longer equal to 1, but rather a smaller value), from which the stimulated emission process can be handled semiclassically. Initially, for an inverted medium, w=1. If nothing perturbs the system, it will remain in this state forever. By introducing the perturbations of spontaneous emissions in the form of tipping angles, the system follows the semiclassical Maxwell-Bloch equations of motion. Since the tipping angle is tied to the initial polarization, the tipping angle also varies in a statistical manner. The problem now is to find the values for the initial tipping angle in a method consistent with the statistics (McCall, 1981).

The distribution of the magnitude of the polarization is based on the QED calculations (Haake et al., 1979a, 1979b; Polder et al., 1979; Haake et al., 1980). It is given by

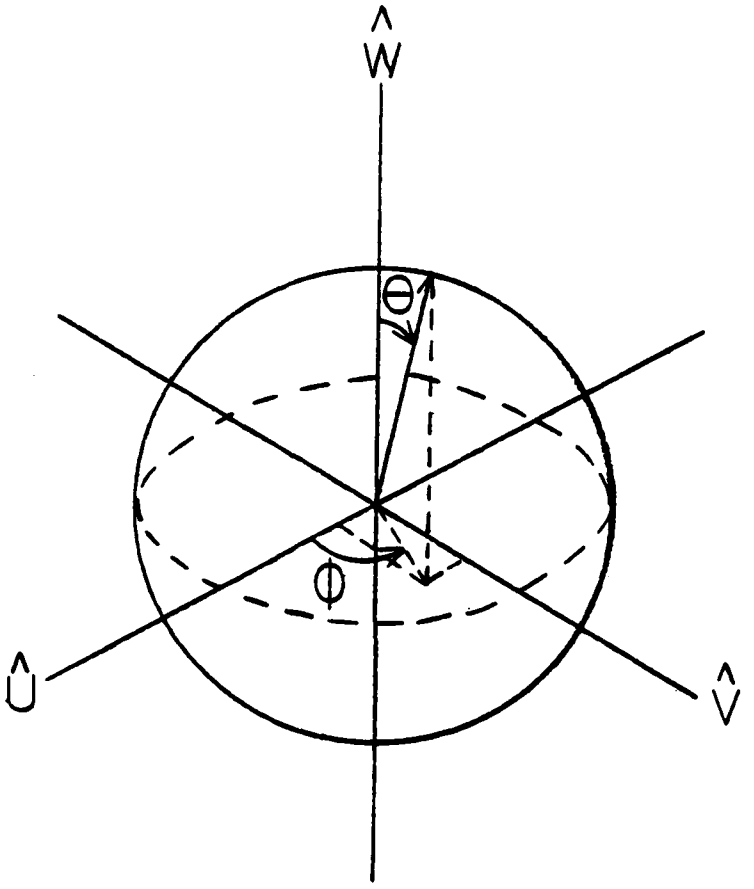

Figure 1. Bloch polarization vector showing the u, v, and w components.

Tipping angle θ and phase angle ϕ are also shown. In the case of no polarization, the vector points along the +w axis.

$$P(u,v)du\ dv = \frac{1}{\pi(4/N)}\ [e^{-(u^2+v^2)/(4/N)}]du\ dv\ , \tag{3}$$

where P is the probability magnitude, u and v are the in-phase dispersive and quadrature absorptive components associated with the Bloch vector, and N is the number of atoms in the sample. Note that the width of the Gaussian goes as 1/N. This expression can be written in a slightly different form as follows. Based on the definition of the Bloch vector,

$$u^2+v^2 = 1-w^2\ . \tag{4}$$

In terms of the tipping angle θ shown in Fig. 1, $w = \cos\theta$. This gives

$$\begin{aligned} u^2+v^2 &= 1 - \cos^2\theta \\ &= \sin^2\theta \\ &\approx \theta^2\ , \end{aligned} \tag{5}$$

for small θ. Hence Eq. (3) can be rewritten as

$$P(\theta^2)d\theta^2 = \frac{1}{4/N}\ e^{-\theta^2/(4/N)}\ d\theta^2\ . \tag{6}$$

Note that the averaged value of θ^2 is given by

$$\langle\theta^2\rangle = \int_0^{\pi} \theta^2\ P(\theta^2)\ d\theta^2 = \frac{4}{N} \tag{7}$$

as specified in the QED calculations. The probability of a tipping angle having magnitude less than or equal to θ_o is given by

$$\int_0^{\theta_o^2} P(\theta^2)d\theta = \frac{1}{4/N} \int_0^{\theta_o^2} e^{-\theta^2/(4/N)} d\theta^2$$

$$= \frac{1}{4/N} (-4/N)\ e^{-\theta^2/(4/N)} \Big|_0^{\theta_o^2}$$

$$= 1 - e^{-\theta_o^2/(4/N)} \quad , \tag{8}$$

which is a number between 0 and 1. Since the tipping angle probability can take on any of these values between 0 and 1, Eq. (8) can be set equal to a random number whose value is between 0 and 1. Equivalently, one can set the value of the exponential equal to a random number between 1 and 0. Then

$$e^{-\theta_o^2/(4/N)} = N_R$$

$$\Rightarrow \frac{1}{N_R} = e^{\theta_o^2/(4/N)}$$

$$\Rightarrow \ell n\ (1/N_R) = \theta_o^2/(4/N)$$

$$\Rightarrow \theta_o = \frac{2}{\sqrt{N}} \sqrt{\ell n\ (1/N_R)} \quad . \tag{9}$$

Eq. (9) gives a method of determining the initial tipping angles in a manner consistent with the distribution described in Eq. (6).

There is another initiation parameter which needs to be considered, and that is the parameter ϕ which was not present in Eq. (6) because the polarization had no special dependence on the ϕ variable

shown in Fig. 1. That is, the Bloch vector could "slide" down any great circle of the sphere. Hence, the value of ϕ can uniformly take on any value between 0 and 2π.

So, the initiation of the superfluorescence pulse can be done by modeling the initial polarization in a statistical manner rather than by considering spontaneous emission. Effectively, this is the same as modeling the system as having deterministic dynamics but with random initial conditions. Then one can deal with the semiclassical Bloch equations rather than the operator equations generated in a completely quantum treatment. It should be noted that the fluctuations in the output which used to be due to the quantum uncertainties are now due to the random nature of the initial polarization. Note also that ensemble averages of the output pulses, both in the experiments and the simulations, correspond to the expectation values obtained using the QED calculations.

Once the initiation process described above has occurred, the remainder of the calculation can be handled semiclassically. This involves using Maxwell-Bloch equations of motion which describe how the first radiation quantum that is emitted down the length of the sample affects the inverted medium. These equations are derived from the density matrix equations of motion which in turn are derived from Schrödinger's equation. The Maxwell-Bloch equations are (Allen and Eberly, 1975; McCall and Hahn, 1969)

$$\dot{u} = \Delta\omega v - \frac{2\mu}{\hbar} w - u/T_2 \qquad (10a)$$

$$\dot{v} = -\Delta\omega u - \frac{2\mu}{\hbar} w E_R - v/T_2 \qquad (10b)$$

$$\dot{w} = \frac{2\mu}{\hbar} v E_R + \frac{2\mu}{\hbar} u E_I - (w+1)/T_1 \qquad (10c)$$

$$\frac{\partial E}{\partial z} - \frac{i}{4FL} \nabla_T^2 E + \frac{n}{c} \frac{\partial E}{\partial t} = -i \frac{2\pi\omega N\mu}{ncV} \int g(\Delta\omega)Q(\Delta\omega)d(\Delta\omega), \qquad (10d)$$

where u, v, and w are the components of the Bloch vector, $\Delta\omega$ is the difference between the applied field and the atomic frequency, E_R and E_I are the real and imaginary parts of the slowly varying complex electric field, T_1 is the decay time from the inverted state, T_2 is the dipole dephasing time, μ is the dipole transition matrix element, $g(\Delta\omega)$ is the lineshape function of the medium, $Q=u(\Delta\omega)-iv(\Delta\omega)$, N is the number of atoms in the medium, V is the volume of the medium, F is the Fresnel number, L is the length of the medium, and n is the background refractive index. For the calculations in this paper, inhomogeneous broadening of the medium was neglected. This was justified since the main purpose was to reproduce the data from an experiment in which inhomogeneous broadening was not significant. Also, it was assumed that $\Delta\omega=0$, i.e. the applied field was on resonance with the atomic line. With thes approximations, $g(\Delta\omega) = \delta(\Delta\omega)$. Eqs. (10) reduce to

$$\dot{u} = - u/T_2 - \frac{2\mu}{\hbar} E_I v \qquad (11a)$$

$$\dot{v} = \frac{-2\mu}{\hbar} E_R w - v/T_2 \qquad (11b)$$

$$\dot{w} = \frac{2\mu}{\hbar} v E_R + \frac{2\mu}{\hbar} E_I u - (w+1)/T_1 \qquad (11c)$$

$$\frac{\partial E}{\partial z} - \frac{i}{4FL}\nabla_T^2 E + \frac{n}{c}\frac{\partial E}{\partial t} = \frac{-i2\pi\omega}{n\,c}\frac{N}{V}\mu\big(u(o)-iv(o)\big) \quad . \tag{11d}$$

Since the field is fast with respect to the atoms, it can be considered to always be in equilibrium. Hence, $\dot{E}=0$. Using this substitution and letting n=inversion density, Eqs. (11) can be further modified to yield (Mattar et al., 1981)

$$\frac{\partial P}{\partial \tau} + \frac{P}{T_2} = \frac{\mu^2}{\hbar} n\, E \tag{12a}$$

$$\frac{\partial n}{\partial \tau} + \frac{n}{T_1} = - \text{Real}(PE^*/\hbar) \tag{12b}$$

$$\frac{\partial E}{\partial z} - \frac{i}{4FL}\nabla_T^2 E = \frac{4\pi^2}{\lambda} P \quad , \tag{12c}$$

where $P=-iN\mu\big(u(o)-iv(o)\big)/V$ is the slowly varying complex polarization amplitude, and $\tau=t-z/c$ is the retarded time. This is the form of the equations used in the present simulations. These equations can be integrated numerically; they then describe the pulse evolution in the sample as a function of the retarded time, the distance along the length of the sample, and the transverse distance.

The following assumptions were made in the calculations performed. First a transverse spatial dependence was assumed in the form of a Gaussian inversion density in the medium. A Gaussian dependence was assumed because the medium in the experiment was initially inverted by a laser. It is this nonuniform density that makes the plane wave solution of the superfluorescence problem only an approximation rather than an exact solution. Radial symmetry was also assumed, i.e., it was

assumed that all directions perpendicular to the direction of propagation were the same. This assumption was made to limit computational time and memory storage. While this assumption eliminates transverse mode competition, the effects should not be significant for Fresnel numbers on the order of one or less. Other work (MacGillivray and Feld, 1976) has shown that interference between forward and backward evolving pulses is very small for the normal circumstances found in most experiments. Therefore, these effects were neglected in this study.

These simulations were done in an attempt to reproduce the results of experiments in superfluorescence done with cesium vapor (Gibbs, Vrehen and Hikspoors, 1977; Vrehen and der Weduwe, in press). Therefore, the material parameters associated with cesium were used. No input pulse was used to start the process, only the statistically modeled quantum initiation was used. Two values of Fresnel number for the beam were used, $F=1$ and $F=1/\pi$.

Discussion of Computer Simulation Program

The program used to produce the simulations of superfluorescence numerically integrated the Maxwell-Bloch equations (Mattar, 1981). The output consisted of curves that showed intensity at the output end of the medium as a function of time and radial distance. Other output curves showed intensity as a function of time by integrating over the transverse dimension. These last curves are what a large aperture detector at the end of the medium would see. The coordinates over which the Maxwell-Bloch equations were solved numerically consisted of the three independent

variables ρ, z, and τ, where ρ was the transverse dimension, z was the longitudinal propagation direction, and τ was the retarded time defined by $\tau=t-z/v$, with v being the speed of light in the medium. The numerical integration was done between specified step intervals in each of these dimensions. In the ρ direction, 29 steps were used, in the z direction, 281 steps were used, and in the τ direction, 64 steps were used. The step size was uniform in the z direction. However, in an effort to minimize computational time and machine memory size required, the step sizes in the ρ and τ dimensions were made nonuniform. By using nonuniform step sizes, it was possible to obtain adequate resolution without encountering excessive machine time and memory requirements. The nonuniform steps were generated in such a way that the step size was minimal in the area around the peak of the superfluorescence pulse, while the step was made large in the calculations of the tail of the pulse. The selective step sizing ensured that maximum calculational effort was made in the areas of interest, while minimal calculations were performed in the areas that were of little significance. Note that in order to make use of this technique, it was necessary to know in advance the areas of interest of the parameters. Hence, this method would not work well if the output would have been completely unknown. The step sizes used are shown in Table 1. As can be seen, the step sizes are smallest in the regions of smallest time and smallest radial displacement. This is appropriate since the fields change most rapidly at small ρ and τ.

Table 1. Value of the grid coordinates in the ρ and τ directions.

There are 29 ρ grid points and 69 τ grid points.

ρ	0.	.1785714E-01	.3574925E-01	.5371171E-01	.7178074E-01	.8999384E-01	.1083983E+00	.1278117E+00
	.1459827E+00	.1651113E+00	.1846985E+00	.2046984E+00	.2252082E+00	.2462694E+00	.2679098E+00	.2901458E+00
	.3137870E+00	.3381099E+00	.3635861E+00	.3904869E+00	.4188178E+00	.4491099E+00	.4816714E+00	.5170855E+00
	.5557933E+00	.5989881E+00	.6479842E+00	.7049417E+00	.7734267E+00			
τ	0.	.1154861E+01	.2306685E+01	.3664434E+01	.4621892E+01	.5781614E+01	.6964193E+01	.8110218E+01
	.9280272E+01	.1045499E+02	.1163498E+02	.1282089E+02	.1401339E+02	.1521315E+02	.1642089E+02	.1763732E+02
	.1886323E+02	.2009939E+02	.2134664E+02	.2260586E+02	.2387796E+02	.2516398E+02	.2646471E+02	.2778147E+02
	.2911532E+02	.3046748E+02	.3183927E+02	.3323209E+02	.3464742E+02	.3608694E+02	.3755227E+02	.3904541E+02
	.4056839E+02	.4212344E+02	.4371300E+02	.4533978E+02	.4700672E+02	.4871710E+02	.5047455E+02	.5228312E+02
	.5414734E+02	.5607230E+02	.5806379E+02	.6012837E+02	.6227355E+02	.6450800E+02	.6684177E+02	.6928663E+02
	.7185658E+02	.7456795E+02	.7744100E+02	.8050809E+02	.8377553E+02	.8730557E+02	.9113936E+02	.9534162E+02
	.1000000E+03	.1052374E+03	.1112336E+03	.1182676E+03	.1268066E+03	.1377269E+03	.1529933E+03	.1780819E+03

After the grid coordinate system was defined, the value of the initial gain coefficient was calculated at each grid point in ρ. The coefficient was generated by

$$G = G_o \, e^{-(\rho/\rho_o)^2} \tag{13}$$

where G_o was the plane-wave gain constant.

With all of the necessary parameters generated, the Maxwell-Bloch equations were integrated numerically. A second order predictor-corrector method was used. The second order method needed the knowledge of the fields and the medium characteristics (u,v,w) in the previous two steps in z. Hence, before an iterative procedure could be used, it was necessary to generate the field and material values in the first two z steps. At the first z step, a routine was called which generated the value of the tipping angle θ_o and the orientation angle ϕ of the Bloch vector in the statistical manner described earlier. Note that now Eq. (9) is replaced by

$$\theta_o^i = \frac{2}{\sqrt{N^i}} \sqrt{\ell n(1/N_R)} \quad , \tag{14}$$

where N^i is the number of atoms in the i^{th} z-ρ grid cell and θ_o^i is the tipping angle for that cell. This ensures that $\langle \theta_o^2 \rangle = 4/N$ as before. Once these values were generated, the Bloch vector components for that particular grid cell were determined from

$$u_o = \sin \theta_o \cos \phi \tag{15a}$$

$$v = \sin \theta_o \sin \phi \tag{15b}$$

$$w = \cos \theta_o \quad . \tag{15c}$$

The values of the medium parameters were then calculated for all time steps at each of the ρ's in the z plane. The derivatives of the radiation field parameters with respect to the spatial coordinates were then calculated. After this, the program moved to the second z step. A similar process was done there, and the program moved to the third z step. At that step, the second order method to predict the values of the fields could be used. From there on out, the process was the same, with the Bloch vector being initialized at each point in the spatial grid using the statistical method. Then the value of the field and medium parameters were calculated for all time at all ρ grid points at a specific z. This process continued until the entire medium had been traversed. At the end of the medium, the values of the field intensity were calculated at each τ and ρ point, and the results were plotted. Then, the field intensity was integrated in the transverse dimension, and a plot of field intensity versus τ for the last z step was made. This would complete one "trajectory," or simulation. The program then could go back to the beginning and repeat the process as many times as requested to output as many trajectories as required.

Results of the Simulations

The first simulations performed were to test the program in the plane-wave case. The results were compared with results of other

plane-wave simulations (Haake et al., 1979a, 1979b, 1980; Polder et al., 1979) that had been performed. The plane-wave case was simulated by setting the number of transverse grid points to 1 and removing the diffraction term from the Maxwell-Bloch Eqs. (12). The results of Haake et al. (1979a, 1979b, 1980) are shown in Figs. 2a, b, c. These results came from simulations (using the parameters of the cesium experiment, Gibbs et al., 1977) in which quantum fluctuations were included but transverse dimensions were not. The quantum fluctuations were introduced through random initial polarizations. Because of the fluctuations, there is not a single delay time, but rather a distribution of delay times. This distribution, Fig. 2c, can be seen to be approximately Gaussian; it consists of 705 trajectories. The distribution has a standard deviation of about 12%. The output for the 705 trajectories was averaged, and the results are shown in Fig. 2b. A typical single trajectory is shown in Fig. 2a. Note the repeated pulsing, called ringing, in Figs. 2a and 2b. This has been explained as follows. The medium is initially in the upper state. As the pulse, which was started from spontaneous emission, propagates through the sample, it stimulates the rest of the medium to radiate cooperatively. However, once the leading edge of the pulse has past a point in the medium, that point is in the ground state and now ready to act as an absorber. The medium absorbs energy from the trailing part of the pulse which re-inverts the medium. The medium then re-radiates, producing the ringing structure. This ringing was first discussed by Burnham and Chiao (1969) and is therefore called Burnham-Chiao ringing. Note that even the

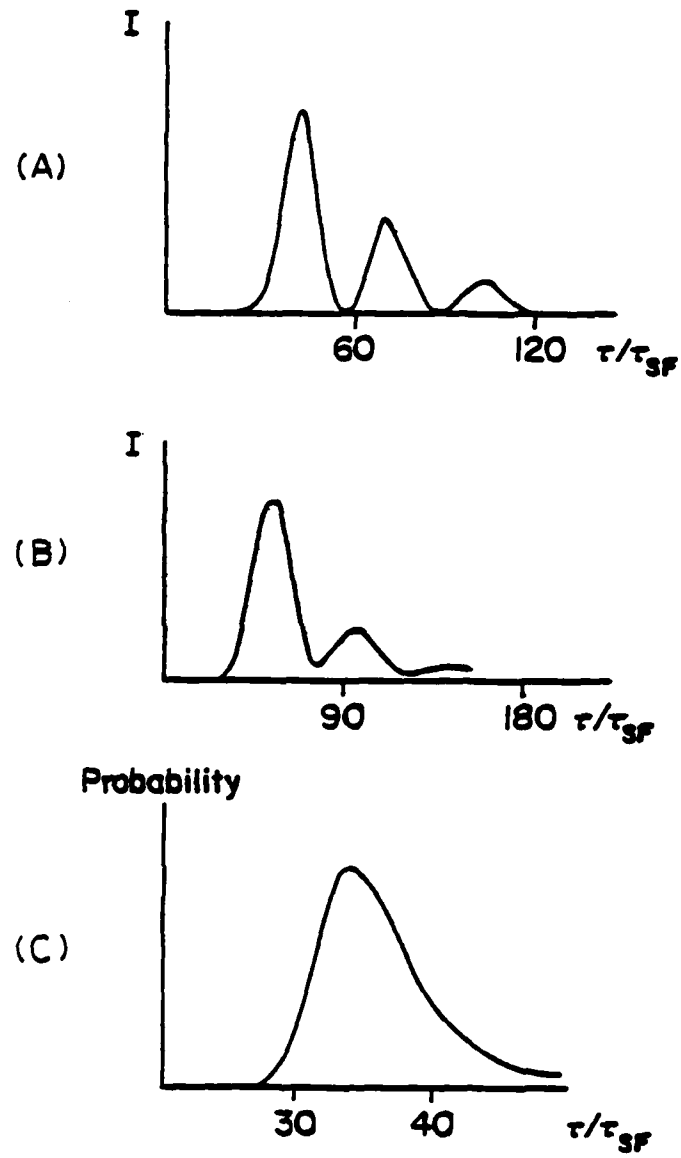

Figure 2. Results of superfluorescence simulations from Haake et al. (1979a, 1979b, 1980).

These results show the effects of quantum fluctuations with no transverse dimension.
(a) Typical single trajectory.
(b) Average of over 700 trajectories.
(c) Distribution of delay times.

average of hundreds of single trajectory pulses does not do much to get rid of the ringing. Hence strong ringing should be observed in a single trajectory. However, the experiments performed by Gibbs et al. (1977) with cesium vapor produced no such ringing structure. It is because of this discrepancy that transverse dimensions are being included in the simulations.

As was stated, the first simulations for this work were done in the plane-wave limit to compare with the previous work. The results of the plane-wave simulations using the cesium parameters are shown in Figs. 3a, b, c. It can be seen that the distribution of delay times, Fig. 3a, is similar to that produced by Haake et al. (1979a, 1979b, 1980). The mean delay time of 57 trajectories is 9.47 ns, and the standard deviation of the distribution is 9.9 ±1.3%, which compares favorably with the 12% standard deviation of the 705 trajectories of Haake et al. Note that a typical single trajectory, shown in Fig. 3b, displays strong ringing and that the average of several trajectories, Fig. 3c, still displays strong ringing. The good agreement between the results from this simulation and those obtained in Haake et al.'s work served as an important check of the statistical and plane-wave aspects of the program. However, the problem of simulated ringing versus no ringing in experimental results still persisted.

To ensure that the program was correctly handling the transverse energy flow, i.e., diffraction, a simulation was run using an "empty cavity." (Actually, this was prompted by some unusual results, as will be discussed more fully later.) The amplifier portion of the program

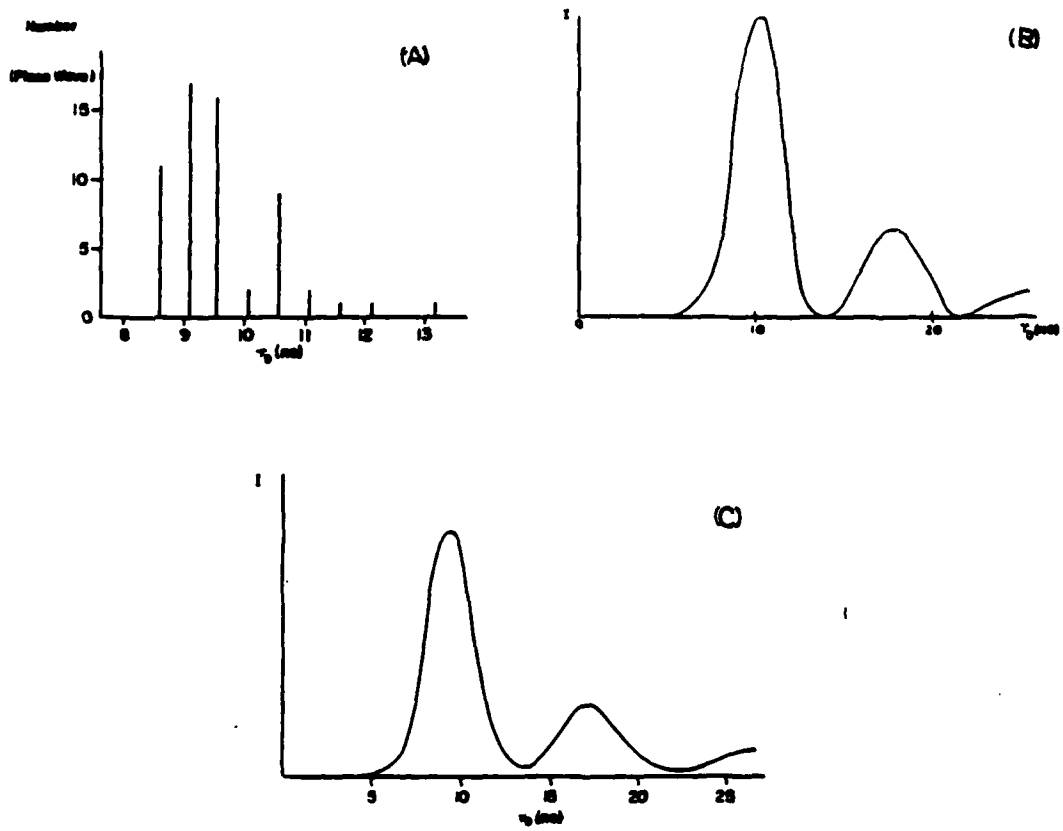

Figure 3. Results of present superfluorescence simulations.

These results show the effects of quantum fluctuations with no transverse dimensions.
(a) Delay time distribution.
(b) Typical single trajectory.
(c) Average of 14 trajectories.

was removed by setting G_o=0. This basically made the medium a cavity in which a pulse could propagate. A sample input pulse was initialized with a known width. The pulse was allowed to propagate the length of the sample, and the width of the output was obtained. The output width was compared with the width the pulse should have assuming that it had propagated according to the standard Gaussian propagation equations. It was found that the widths compared to within 1%. Therefore, it appeared that the diffraction effects were being handled properly in the program.

The first run with transverse dimensions included in the calculations was made without using quantum fluctuations. The results then could be compared with previous simulations performed by Mattar et al. (1981). The fluctuations were removed by assuming that every spatial grid coordinate had the same initial tipping angle and orientation angle. A Fresnel number of one was used to correspond with the earlier work. The parameters of the cesium experiment, except for one, were used in the simulation. The one parameter not matched with the experiment was the inversion density. Mattar et al. (1981) have shown that the cesium data could be better reproduced by using a density of n = $1.8*10^{11}$ atoms/cm^3 rather than the experimental value of $7.6*10^{10}$ atoms/cm^3 (+60%, -40%). This convention was therefore adopted. The results of this simulation are shown in Fig. 4a. Mattar et al. results are shown in Fig. 4b. Comparison of the two figures shows very similar results. It can be seen that with just the inclusion of the transverse dimension and no fluctuations the amount of ringing is greatly reduced in the integrated plot, while the ringing is still strongly present

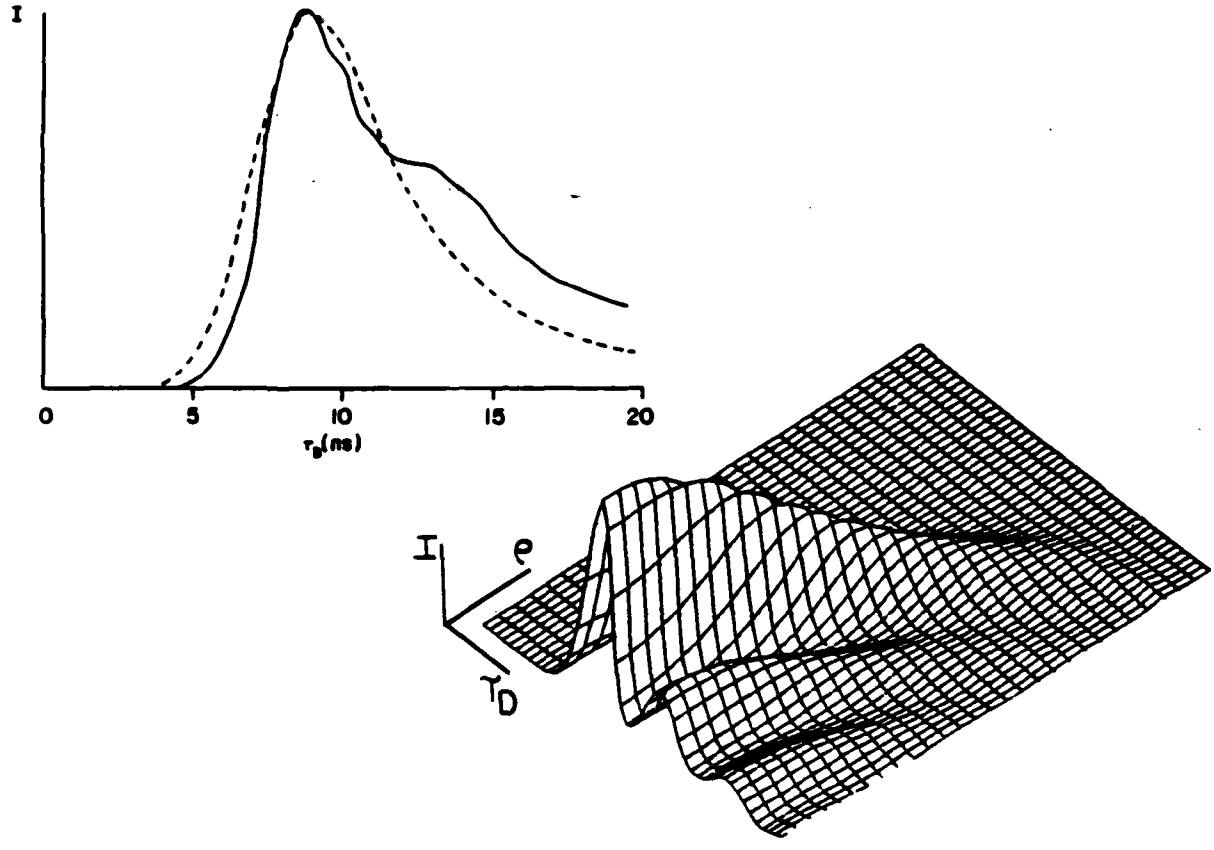

(a)

Figure 4. Results of simulation with transverse dimensions but no quantum fluctuations, Fresnel number equal to 1.

(a) Results of simulations performed for this paper. Upper curve is the integration of the lower curve over the transverse dimension. The dotted line represents data from the cesium experiment in Gibbs, Vrehen and Hikspoors (1977). Note the strong ringing on-axis in the 3-dimensional plot.

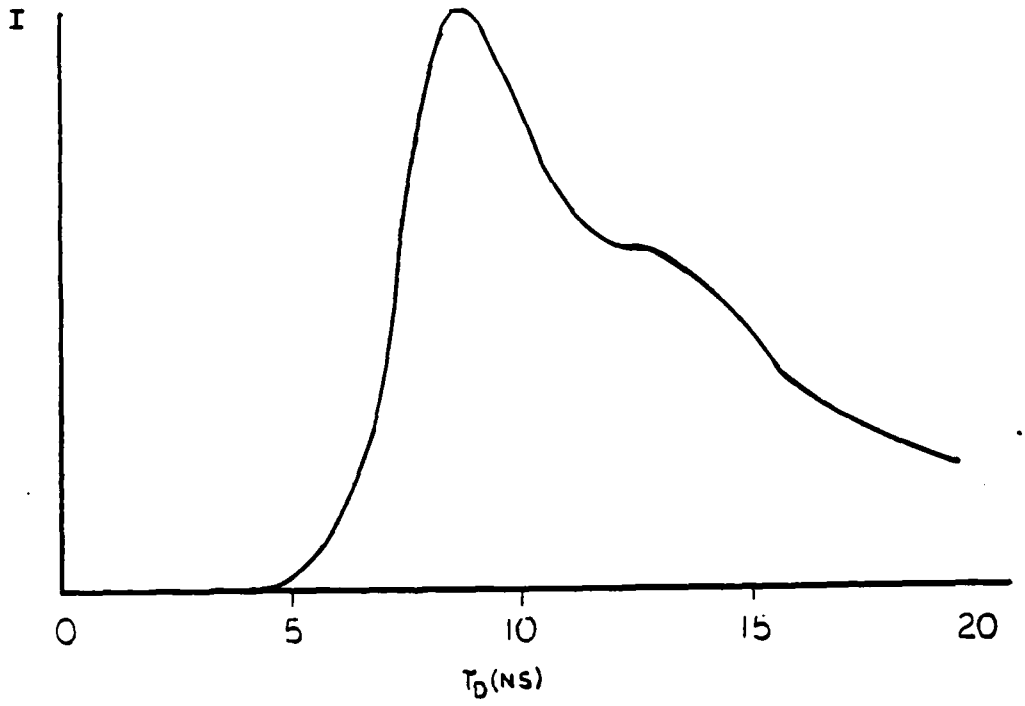

(b)

Figure 4.--Continued

(b) Results of simulations reported in Mattar et al. (1981). These results obtained by integrating over the transverse dimension.

on-axis in the 3-dimensional plot. Hence, a large aperture detector would see little ringing while a small detector in the center of the output beam would see strong ringing.

Next, simulations were run including both transverse dimensions and quantum fluctuations. Figures 5a-d show several of the 12 trajectories that were made with Fresnel number=1. The curves are linear plots of the nonlinear mesh given in Table 1. Therefore, the size between neighboring steps in ρ and τ are not uniform. Note first that the 3-dimensional curves are no longer smooth in the transverse direction as the no-fluctuation curve was. It is hypothesized that the rapid transverse variations were due to the random statistics of the polarization and the fact that, for Fresnel number=1, diffraction is not strong enough to couple strongly the individual annular rings modeled in the program. (It was at this point that the diffraction test discussed earlier was done to ensure that the program was handling it properly.) To further test the hypothesis, it was decided to make some runs with Fresnel number of $1/\pi$. By using this smaller Fresnel number, the beam would correspondingly have a smaller diameter, which would increase diffraction. It was hoped that the increased diffraction would couple the individual rings more strongly, thereby reducing the transverse variations. It is not believed that the transverse variations affect the time delays or the integrated plots. Before going on to the $F=1/\pi$ results, a few more points need to be made for the F=1 case. It can be seen in Figs. 5a-d that the strong ringing that was prevalent in the 3-dimensional plots of the no-fluctuations case is reduced. Also it can

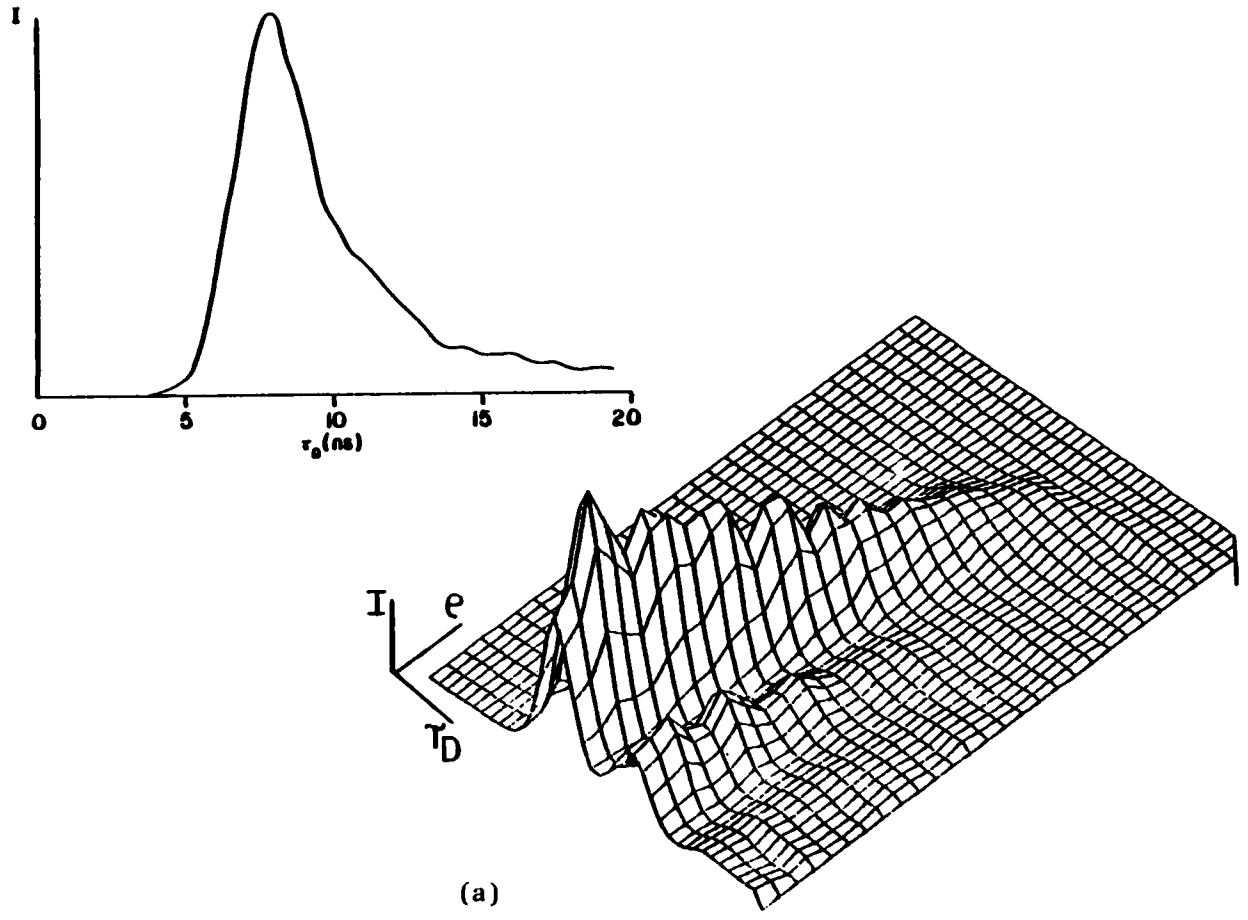

(a)

Figure 5. Typical trajectories for simulation with both transverse dimensions and quantum fluctuations included, Fresnel number=1.

(a) Initial polarization as described in text.

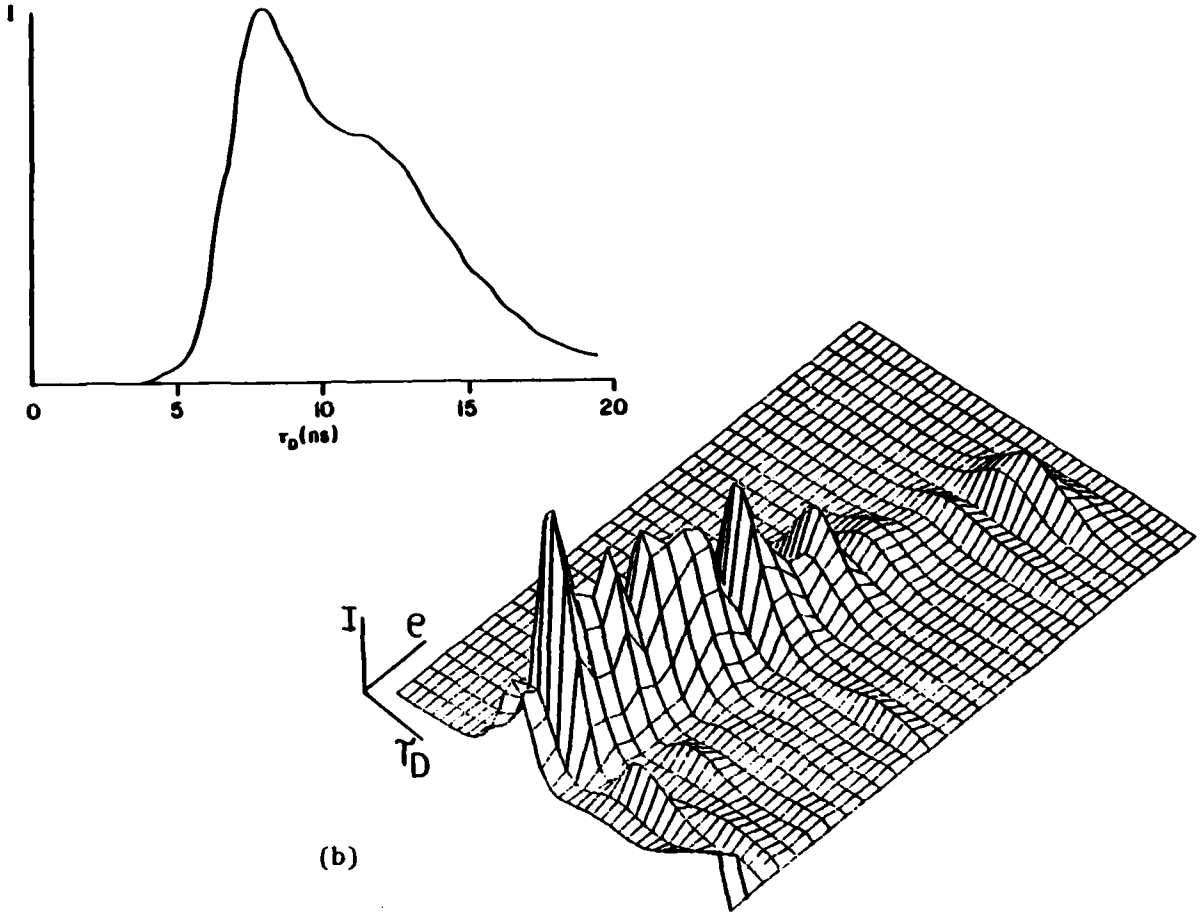

(b)

Figure 5.--Continued

(b) Same conditions as in (a) except initial polarization.

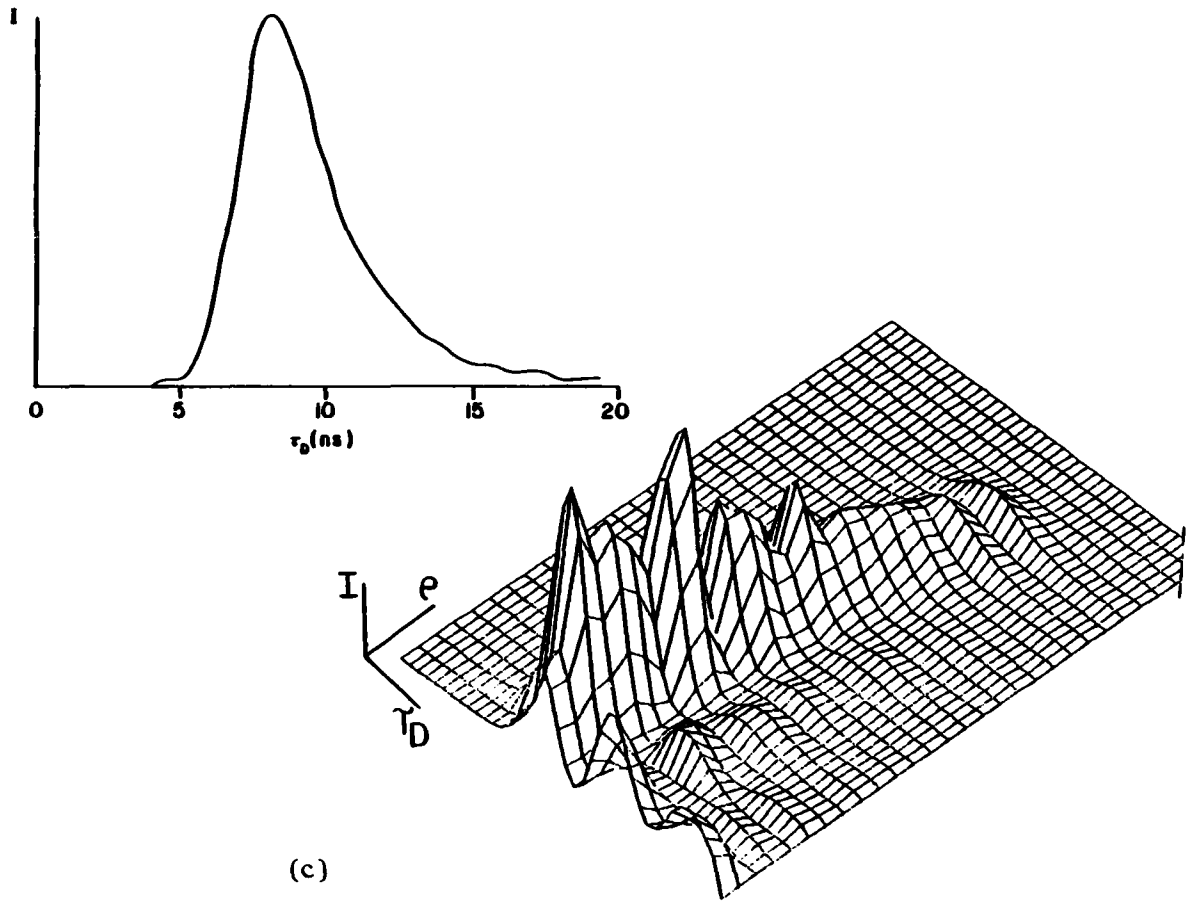

(c)

Figure 5.--Continued

(c) Same conditions as in (a) and (b) except different initial polarization.

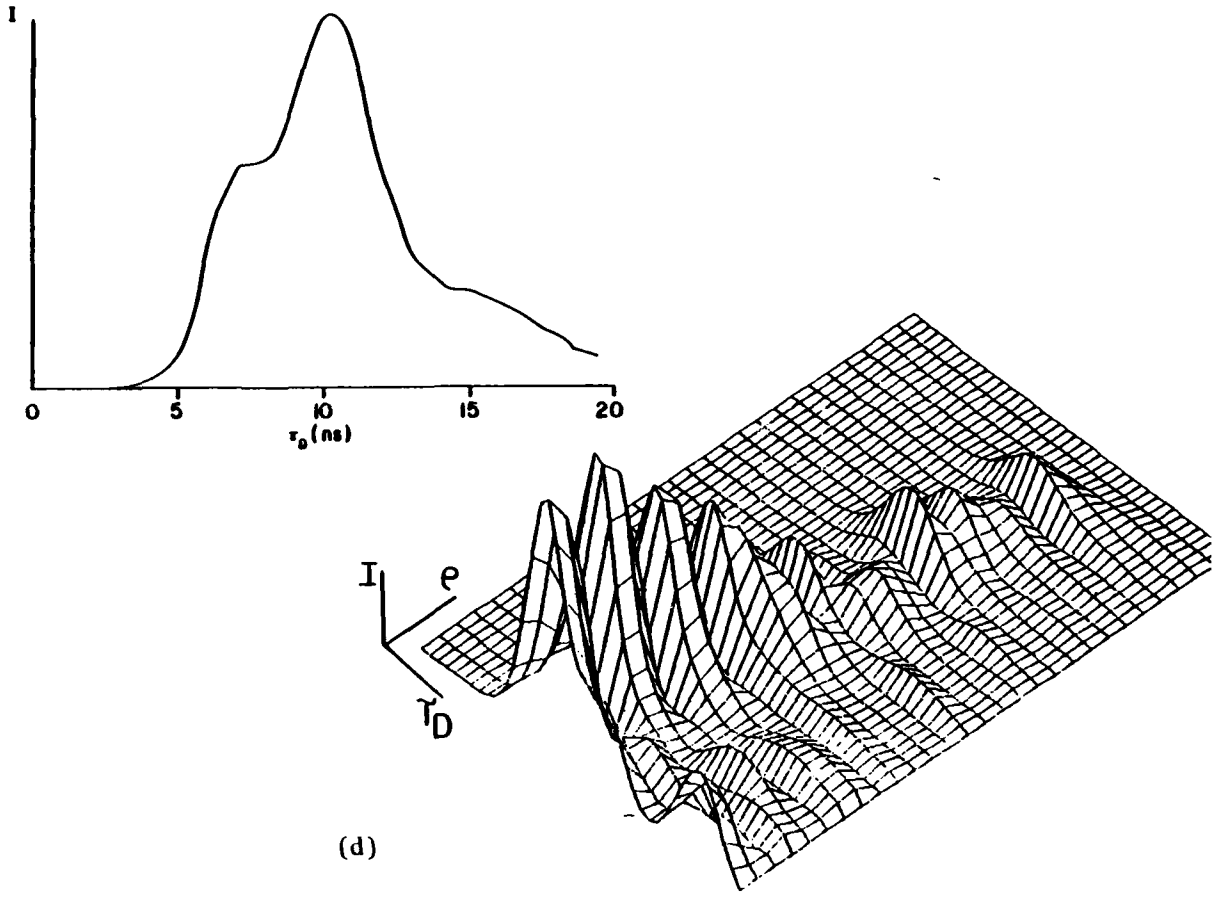

(d)

Figure 5.--Continued

(d) Same conditions as in (a), (b), and (c) except for different initial polarization.

be seen that in most trajectories, the integrated output curves have significantly reduced tails with less ringing evident than in the no-fluctuation case. In several trajectories, the pulse is very nearly symmetrical. This agrees well with the results of the cesium experiments in which symmetrical pulses were frequently seen, as well as pulses with larger tails. The average time delay for the 13 runs of the F=1 case was 7.9 ns with a standard deviation σ=1.03 ns (see Fig. 6). This compares favorably with the experimental value of 9.1 ns.

Similar results are shown for the F=1/π case in Figs. 7a-d and Fig. 8. Figure 7a shows the no-fluctuations case for this Fresnel number, and Figs. 7b through d show various typical trajectories of the 16 runs for this Fresnel number. As was predicted, the transverse variations in the output profile were reduced by increasing the diffraction. Hence, it would appear that if a finer radial mesh were used in all the calculations, the rapid transverse variations would disappear, leaving more slowly varying transverse changes that would be physically significant. The average delay time for the F=1/π case is 9.3 ns with σ=.671 ns (see Fig. 8).

Figures 6 and 8 show the delay distribution for the calculations performed, F=1 and 1/π respectively. The results are:

σ=13.0 ±3.6% F=1

σ=7.2 ±1.8% F=1/π

These results compare with 10 ±2% measured by Vrehan and der Weduwe for the F=.8 case in recent experiments with cesium vapor.

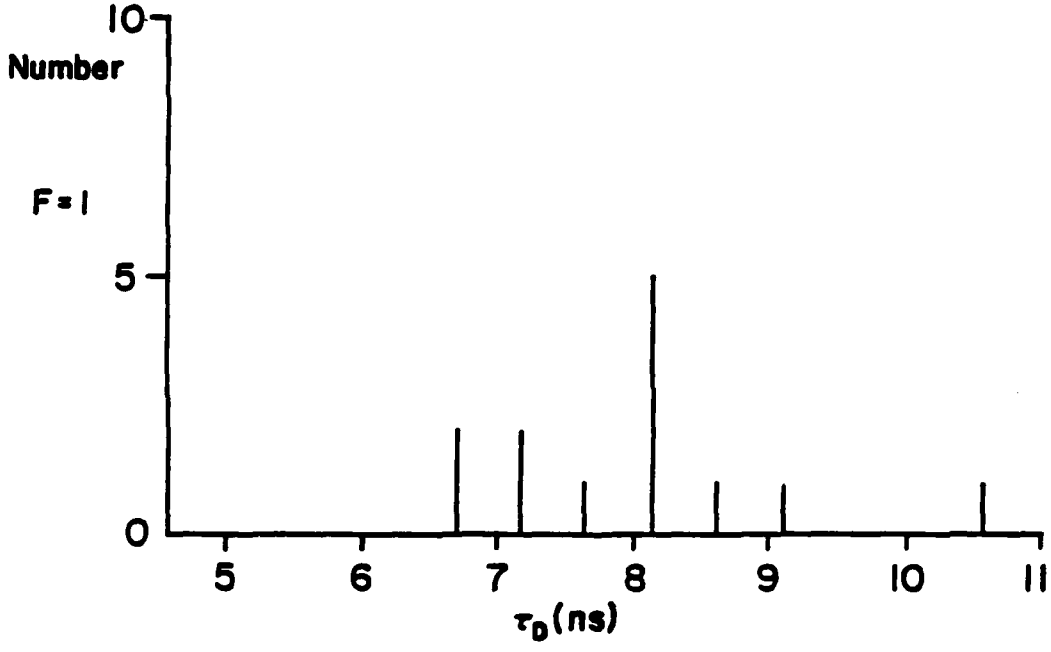

Figure 6. Delay time distribution for the Fresnel number=1 case.

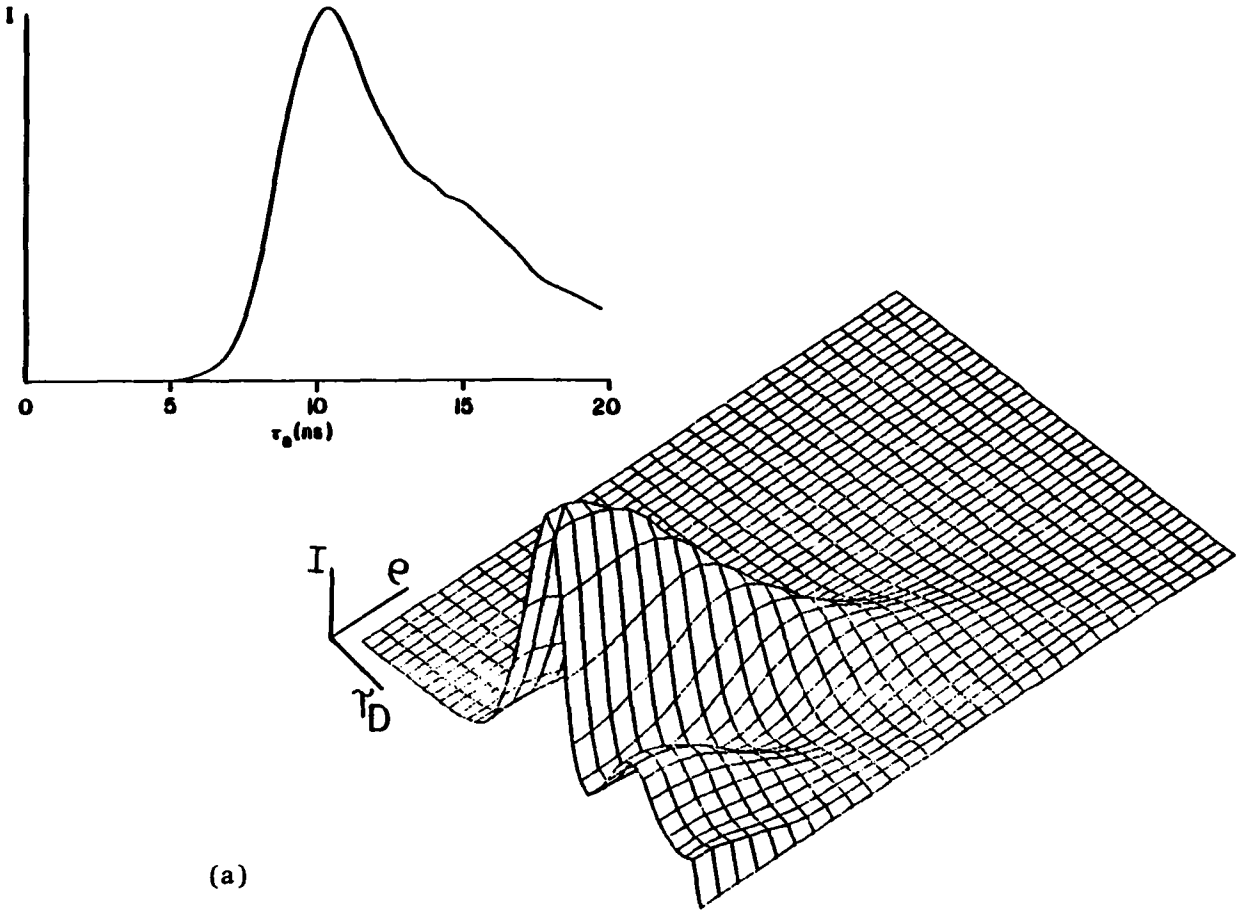

(a)

Figure 7. Results of simulation with transverse dimensions for the Fresnel number=$1/\pi$ case.

(a) No quantum fluctuations included.

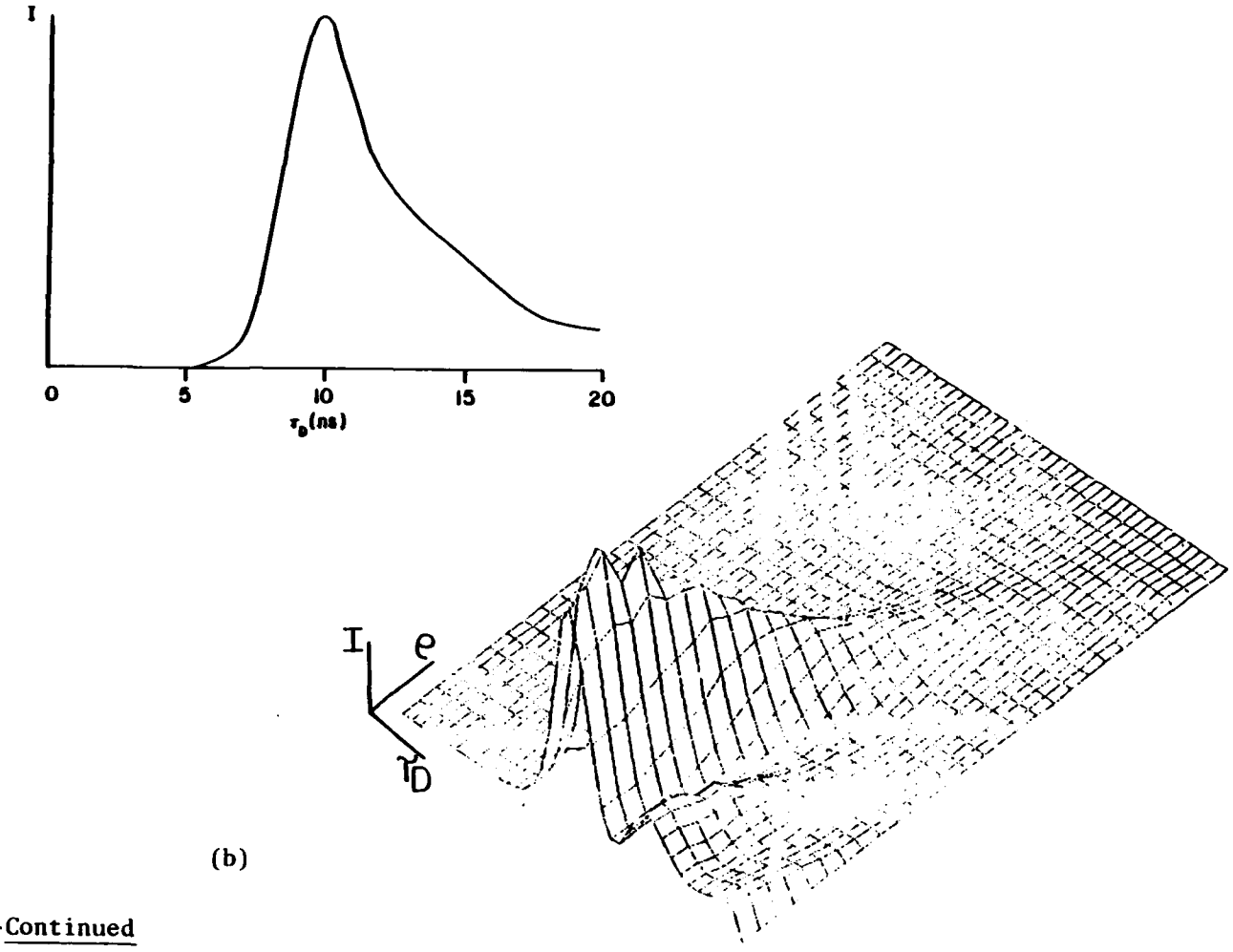

(b)

Figure 7.--Continued

(b) Quantum fluctuations included.

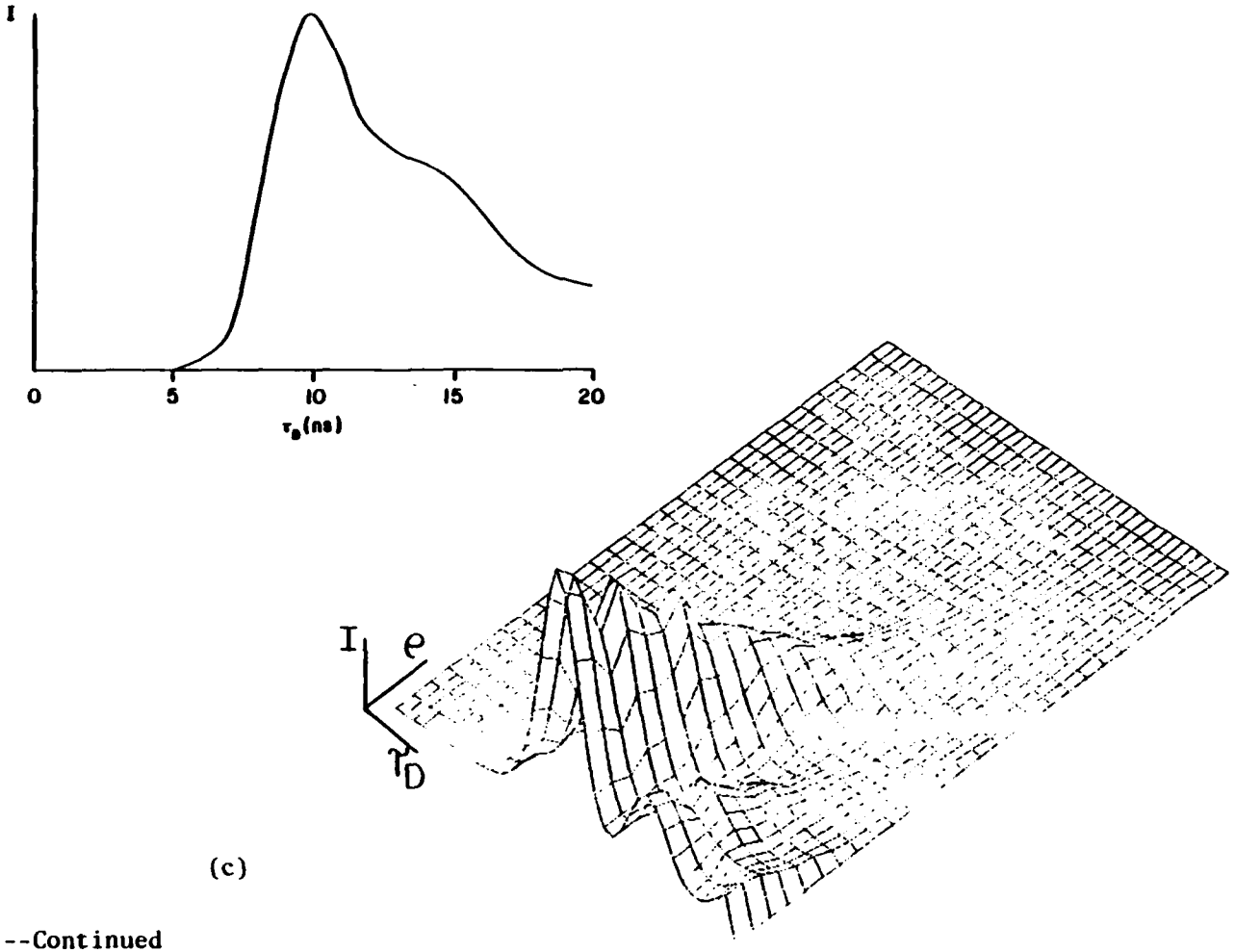

(c)

Figure 7.--Continued

(c) Same conditions as in (b) except different initial polarization.

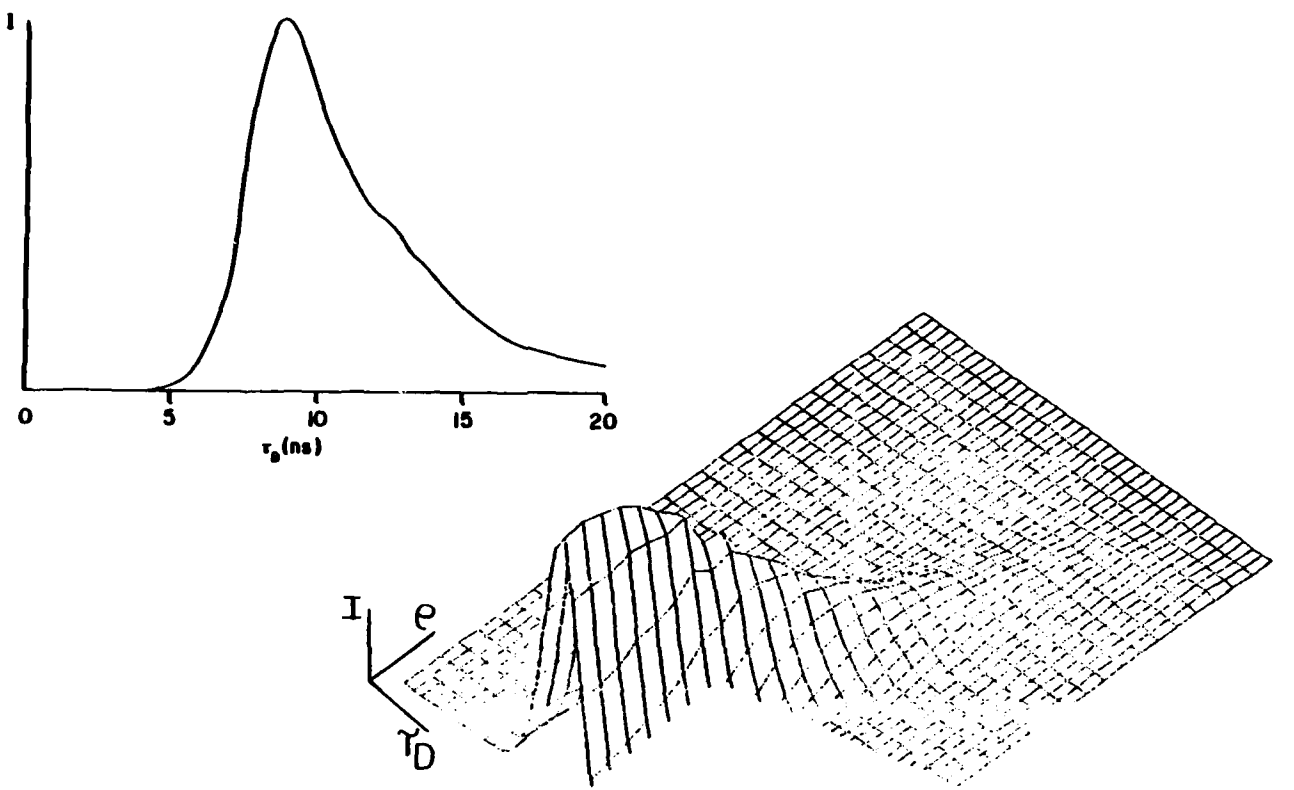

(d)

Figure 7.--Continued

(d) Same conditions as in (b) and (c) except different initial polarization.

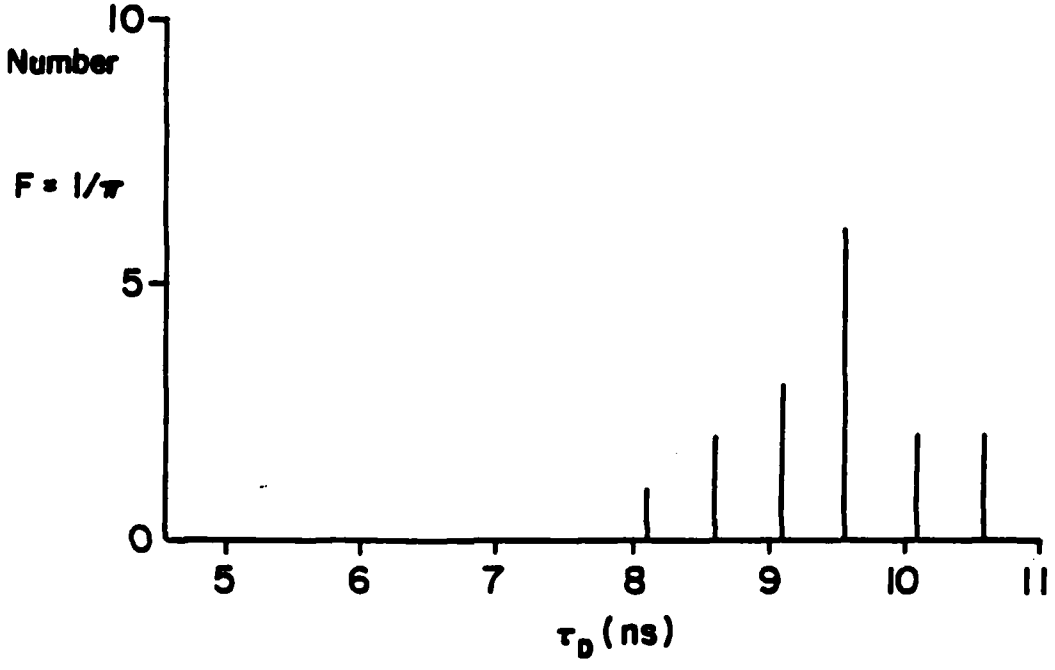

Figure 8. Delay time distribution for the Fresnel number=1/π case.

Conclusions

Experiments in superfluorescence using cesium vapor have shown single-pulse output with a distribution of delay times. Simulations using quantum fluctuation statistics alone predicted a strong ringing structure, and also agreement with the experimental data was not very good. Simulations using transverse effects alone showed no ringing and agreement with the experiments was good. However, the tails of the simulation output pulses were too long. The simulations using both transverse effects and quantum fluctuations presented here achieve better agreement than transverse effects alone in that the tails are reduced. The distribution of delay times agree favorably with the distributions obtained in experiments. The good agreement is consistent with other studies indicating two-way pulse propagation effects and inhomogeneous broadening effects are small for the cesium experiment. The physics of the superfluorescence pulse and its fluctuations now seems well understood.

CHAPTER 3

OPTICAL BISTABILITY SIMULATIONS

Background

Simply stated, optical bistability deals with optical systems which exhibit the characteristic that for a given input intensity, the device has two stable output intensities. Optical bistability is a relatively new field of optics. It is receiving a great deal of attention, however, for several reasons. One reason is that it is an interesting physical problem. It is also a problem that has several possible practical applications (Gibbs, McCall and Venkatesan, 1976, 1979, 1980; Gibbs et al., 1979; McCall, 1978; McCall and Gibbs, 1978; McCall et al., 1975; Shank, Ippen and Shapiro, 1978; Smith and Tomlinson, 1981; Smith, Turner and Maloney, 1978; Smith and Miller, 1981; Miller, Smith and Johnston, 1979; Venkatesan and McCall, 1977). Some of these applications are as an optical memory, an optical discriminator, an optical transistor, and, in combinations, as an optical flip-flop. Hence, the potential is very good for these devices to create all optical systems. It is primarily for this reason that the subject is receiving so much attention.

There are two basic types of optical bistability; these are absorptive bistability and dispersive bistability. While the details of the phenomena are different in each case, both have two things in common.

In each case, the device must have some kind of feedback in order to achieve bistability. Also each type depends on the nonlinear interaction of light with some medium to produce the bistable effect.

Absorptive bistability depends on the ability of the medium to be saturated. The bistability results from the fact that the absorption characteristics of the medium depend upon the intensity of the field in the medium. Consider as an example of such a device a Fabry-Perot cavity filled with some sort of saturable medium. The equation governing the transmission through such a cavity is

$$\frac{I_t}{I_i} = \frac{e^{-\alpha L/\cos\theta}\,(1-R-A)^2}{(1-R')^2\left[1 + \frac{4R'}{(1-R')^2}\sin^2\frac{\delta}{2}\right]} \quad , \tag{16}$$

where I_t is the transmitted intensity, I_i is the input intensity, R is the reflectance of the cavity mirrors (assumed to be the same for each mirror), A is the loss due to interactions at each surface, T is the transmittance, αL is the absorption in one pass through the cavity, θ is the angle that the light makes with respect to the mirror normals inside the cavity, δ is the round trip phase shift, and $R' = R\, e^{-\alpha L/\cos\theta}$. For saturable absorbers, αL depends upon the intensity of the field in the cavity. For a homogeneously broadened medium, the dependence is given by

$$\alpha L = \frac{\alpha_o L}{1 + I/I_s} \quad , \tag{17}$$

where $\alpha_o L$ is the zero field value for the absorption per unit length, and I_s is the saturation intensity.

Initially, when a field is first applied to the device, $\alpha L=\alpha_o L$, which can be large enough to not allow much transmission as determined by Eq. (16). As the input intensity increases, the value of αL decreases causing a corresponding increase in I_t. Under certain conditions, the device rapidly becomes highly transmitting. The device is said to "turn on," or "switch up." If, after the device is turned on, the input intensity is lowered slowly, the reverse of the above happens; the device "switches off." However, switch off does not occur at the same intensity as switch on. Since the transmission was high, the intracavity intensity I_t/T was very large since $I_t \approx I_i$. Thus there is considerable intensity in the device. This intensity does not let the medium "unsaturate" as quickly as it saturated. The device remains highly transmitting so that most of the input gets into the cavity, even for input intensities that were poorly transmitting in the earlier case. A plot of such an experiment would yield the familiar hysteresis curve shown in Fig. 9.

Dispersive bistability works in a similar fashion to the process just described; however, it depends on a medium with a nonlinear index of refraction rather than a saturable absorption. Initially, the device and the input (usually a laser) are detuned. Therefore the device is fairly low transmitting, depending upon the detuning and the finesse of the device. Figure 10 shows I_t as a function of frequency for R=.5. Now, the complex susceptibility of the intracavity medium is given by

$$\chi = \frac{1 + i\Delta\omega T_2}{1 + I/I_s + (\Delta\omega T_2)^2} \quad . \tag{18}$$

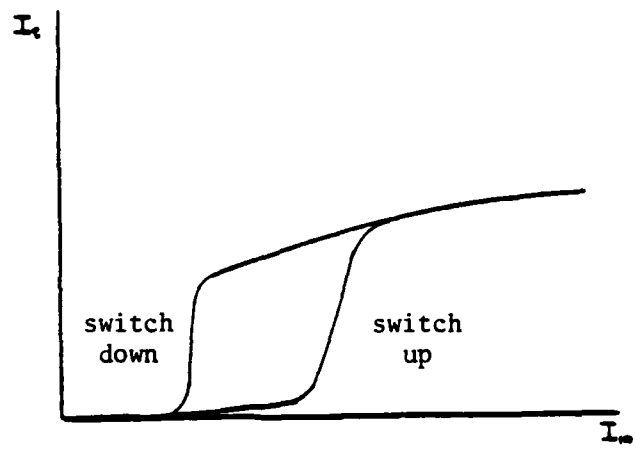

Figure 9. Hysteresis loop depicting optical bistability.

Note the rapid changes of intensity at the switch-up and switch-down points.

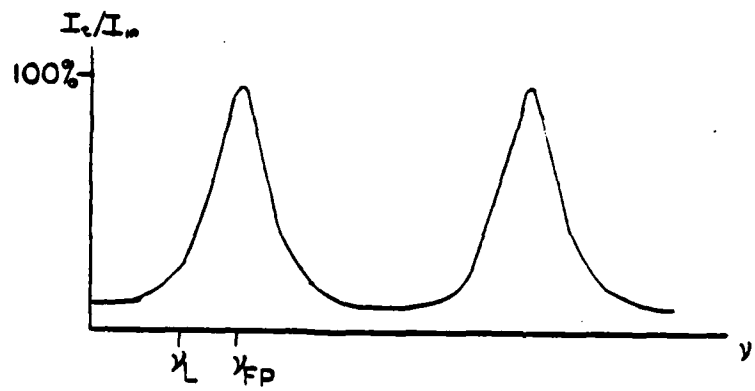

Figure 10. Transmission of a Fabry-Perot cavity as a function of frequency.

Initially the frequency of the laser ν_L is detuned from the peak transmission of the cavity ν_{FP}. Because of the nonlinear medium in the cavity, the value of ν_{FP} will shift as the input intensity changes, thereby allowing the transmitted intensity to change.

Hence, as the intracavity field intensity changes, so does the optical path length in the cavity. This in turn changes the frequency that the cavity transmits highly. As the cavity intensity rises, the peak transmission frequency is moved until it moves just beyond the input frequency, at which point the device becomes highly transmitting. If the input intensity is slowly decreased, the peak transmission frequency again begins to shift. However, because of the large intracavity intensity, the peak does not shift away (turn off) at the same intensity as it switched on. The large intracavity intensity keeps the index shifted from its zero-field value. The result is to again trace out a hysteresis loop similar to the one in Fig. 9.

Model of Optical Bistability

The model of optical bistability used (Bonifacio and Lugiato, 1976, 1978a, 1978b; Bonifacio, Gronchi and Lugiato, 1979; Gronchi and Lugiato, 1980) contains both the absorptive and the dispersive effects just discussed. Since optical bistability deals with matter-light interactions, just like superfluorescence, the same coupled Maxwell-Bloch equations can be used to describe the phenomena (see Eqs. 10). Following the notation suggested in the work done by Bonifacio and Lugiato, the following substitutions are made:

$$P(\Delta\omega) = \frac{N(\Delta\omega)}{2} [v(\Delta\omega)+iu(\Delta\omega)]$$

$$\Delta = \frac{-Nw}{2}$$

$$E = \sqrt{2}\, E$$

$$\eta = 1$$

$$\gamma_{11} = 1/T_1 \; ; \quad \gamma_1 = 1/T_2$$

$$g = 4\pi\omega_o\mu/V \quad , \tag{19}$$

where P is the complex polarization, Δ is the population difference, N is the total number of atoms in the medium, and V is the volume. With these substitutions in Eqs. (10) the Maxwell-Bloch equations become

$$\dot{P} = \frac{\mu E \Delta}{\hbar} - (\gamma_1 - i\Delta\omega)P \tag{20a}$$

$$\dot{\Delta} = \frac{\mu}{\hbar}(EP^* + E^*P)/2 - \gamma_{11}(\Delta - N/2) \tag{20b}$$

$$\dot{E} + C\frac{\partial E}{\partial z} - \frac{i}{4FL}\nabla_T^2 E = -g\int P(\Delta\omega)g(\Delta\omega)d(\Delta\omega) \tag{20c}$$

These equations can be readily solved in the steady state. In this case, $\dot{P}=\dot{E}=\dot{\Delta}=0$. Then Eqs. (20) take on the form of

$$\Delta(\Delta\omega) = \frac{N(\Delta\omega)}{2}\,\frac{1 + (\Delta\omega/\gamma_1)^2}{1 + X^2 + (\Delta\omega/\gamma_1)^2} \tag{21a}$$

$$P(\Delta\omega) = \frac{N(\Delta\omega)}{2}\left(\frac{\gamma_{11}}{\gamma_1}\right)^{1/2}\frac{(1 + i\Delta\omega/\gamma_1)X}{1 + X^2 + (\Delta\omega/\gamma_1)^2} \tag{21b}$$

$$\frac{dX}{dz} = \frac{-\alpha_o}{2} X X_I \quad , \tag{21c}$$

where

$$X = \frac{\mu/\hbar}{\sqrt{\gamma_{11}\,\gamma_1}} E \quad ;$$

$$\chi_I = \int g(\Delta\omega) \frac{1+i\Delta\omega/\gamma_1}{1+\chi^2+(\Delta\omega/\gamma_1)^2} \, d(\Delta\omega) \quad ;$$

$$\alpha = \frac{\mu}{\hbar\gamma_1} \frac{1}{C} \frac{4\pi\omega_o\mu}{V} \frac{N}{2} \quad .$$

The wave equation, Eq. (21c), can be simplified for the present case. Considering a homogeneously broadened medium, then the shape factor $g(\Delta\omega)$ is defined as:

$$g(\Delta\omega) = \delta(\Delta\omega-\Delta\omega^\circ) \quad . \tag{22}$$

In this case, Eq. (21c) can be modified to

$$\frac{dX}{dz} = \frac{-\alpha_o}{2} \chi \, X \quad , \tag{23}$$

where χ is defined as

$$\chi = \frac{1+i\Delta\omega^\circ/\gamma_1}{1+(\Delta\omega^\circ/\gamma_1)^2+\chi^2} \quad . \tag{24}$$

If the field in the cavity is assumed to be slowly varying over a small interval ΔL, then Eq. (23) can be integrated by assuming $X(z) \approx X(L) =$ constant. Then,

$$X(L+\Delta L)-X(L) \approx \frac{-\alpha_o}{2} \chi \, L \, X(L) \tag{25a}$$

$$X(L+\Delta L) \approx X(L) + \frac{-\alpha_o}{2} \chi \, L \, X(L) \tag{25b}$$

$$\approx X(L)\left[1 + \frac{-\alpha_o}{2} \chi \, L\right] \quad . \tag{25c}$$

Equation (25c) gives a method to find the fields in the cavity while propagating through an absorptive/dispersive medium.

Program Used in Calculations

The assumption was made that the medium responds quickly with respect to the field. In this limit, the atoms instantaneously follow the field. Hence the atomic parameters (u,v,w) can be eliminated. The Maxwell-Bloch equations reduce to just the propagation Eq. (25c). The simulations were done for the case of a ring cavity so that standing-wave effects could be ignored.

The geometry of the cavity is shown in Fig. 11. The program used (Belic, 1979; Lax, Louisell and McKnight, 1975; Agrawal and Lax, 1979) to propagate the fields through the cavity can be broken into three basic parts. The first is the free space propagation of the input field to the nonlinear medium. The second part is the propagation through the medium. The last part is the free space propagation back to the start of the ring cavity.

The free space propagation follows the wave equation, in the steady state, of

$$\frac{\partial E}{\partial z} - \frac{i}{4FL} \frac{\partial^2}{\partial x^2} E = 0 \quad . \tag{26}$$

Note that only one transverse dimension was used in the calculations. To solve Eq. (26), the Fourier transform is taken with respect to the transverse coordinate. The equation is solved in the transform space for the transverse coordinate, and then the inverse transform is used to get the result back to normal spatial coordinates. The result is that computer core storage and computational time are greatly reduced. This method is made rapid by using Fast Fourier Transform methods.

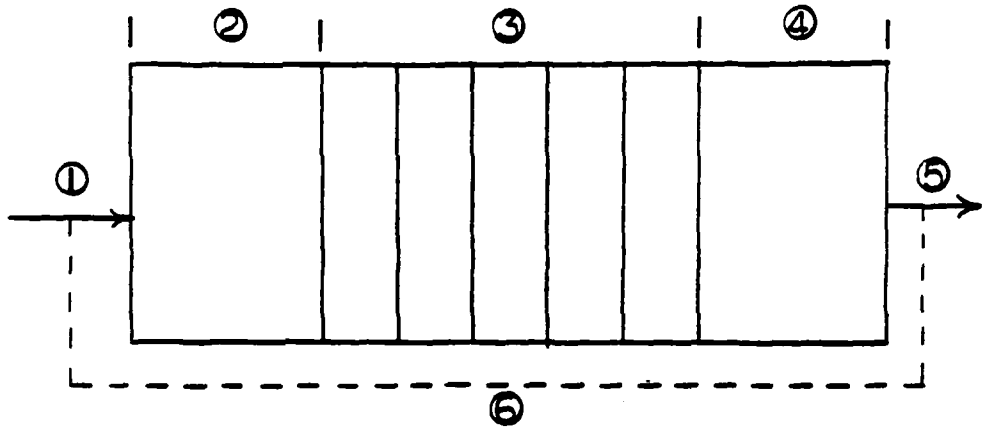

Figure 11. Geometry of ring cavity used in the simulations.

1. Field at the left hand mirror is made up of the input field and the field reflected from the right hand mirror and free space propagated back to the left hand mirror.
2. Free space propagation of the field to the non-linear medium.
3. Stepping through the medium by modifying the field at each medium sheet and free space propagating between the sheets.
4. Free space propagation of the field to the right hand mirror.
5. The field leaving the right hand mirror is partially transmitted and partially reflected back to the left hand mirror.
6. Free space propagation of the field from the right hand mirror to the left hand mirror.

The medium propagation can be handled in much the same way as the free space propagation if the following addition is made. It is assumed that the medium can be represented by a series of very thin gain sheets separated by free space. Then, the free-space propagator can be used to propagate between the sheets, each of which essentially take no space in the propagation direction. At each gain sheet, the fields are modified using Eq. (25c). Hence, there is free space propagation from the input plane to the first gain sheet located, say, at z_o. Then, the fields are modified using Eq. (25c). They free-space propagate to the next gain sheet, a distance Δz away. Then Eq. (25c) is used again to determine the field $E(z_o+\Delta z)$ from $E(z_o)$. This process is repeated until the entire medium is traversed. Then the fields at the end of the medium are free space propagated back to the input plane where they are modified by additional input. The entire procedure continues until the cavity reaches a steady state. When this occurs, the values of the input and the output are recorded for each transverse coordinate for future plotting. Then the value of the input is incremented and the process repeats itself. The program loops through a specified number of input values, then, after having reached the maximum input value, it descends back down the input values. In this way, the bistability loop can be traced out. After all the input points have been processed, the bistability loops at specified transverse points are plotted out. Also, a loop in which the input and output have been integrated over the transverse dimension is also plotted out.

Results of the Calculations

The basic purpose of these calculations was to investigate how far a bistable device turns on in the transverse direction. Since most of the work to date has been done for plane-wave input, the questions of how much of the device becomes bistable and what effect diffraction has have not been answered. One would expect that the Fresnel number of the system would play an important role because of its presence in the diffraction term in Eq. (26). Because of the Fresnel number dependence, calculations were run at several Fresnel numbers. The Fresnel number is defined as $\rho^2/\lambda L$, where ρ is the half-width at half maximum of the input beam, λ is the wavelength of the input, and L is the length of the sample through which the beam travels. Now, since the beam is in a cavity, the value of L is not just the length of the cavity, but rather the length which the beam travels in the cavity. Since the beam makes several passes, the total length the beam travels is actually several times the length of the cavity. A measure of the number of passes that the beam would make is given by the finesse of the cavity, defined as $\pi\sqrt{R}/(1.-R)$, where R is the reflectance of each of the two mirrors, assumed to be equal. Then for a cavity with $R \approx .9$, the finesse is $\mathcal{F} \approx 30$. Using an effective Fresnel number defined as $\rho^2/\lambda L'$ where L'= finesse*length of cavity, the calculations were performed for effective Fresnel numbers of .002, .02, .2, 2., and 20.

The results presented here are meant to be mostly qualitative, indicating trends rather than actual values. Figures 12a, b, c, d, e show the transmitted field as a function of the input field to the

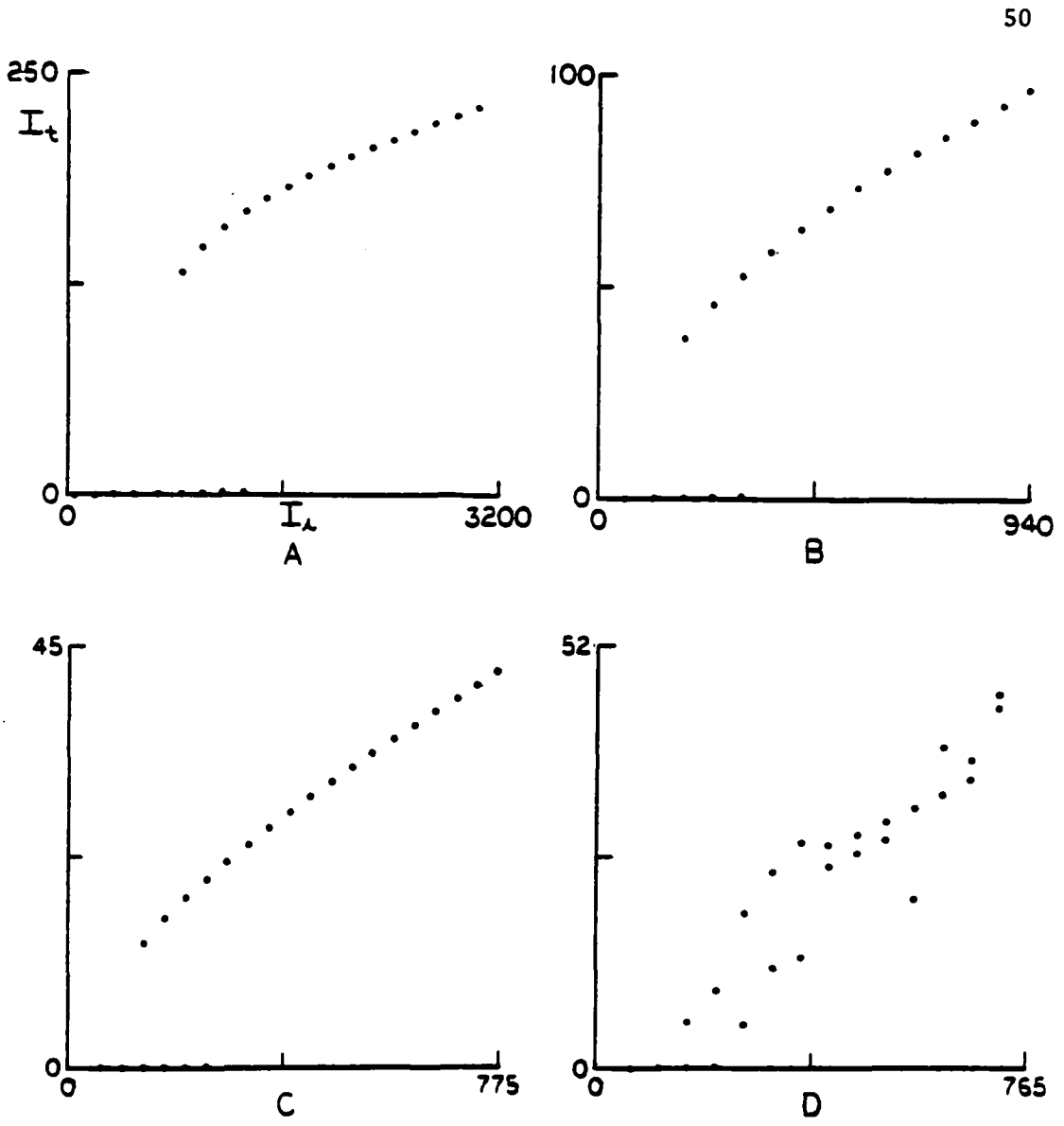

Figure 12. Results of simulations of optical bistability including transverse dimensions.

Plots show output intensity integrated over the transverse dimension as a function of the input intensity integrated over the transverse dimension.

(a) Fresnel number=.002.
(b) Fresnel number=.02.
(c) Fresnel number=.2.
(d) Fresnel number=2. The curve is not smooth because the cavity had not reached steady state when the calculations stopped.

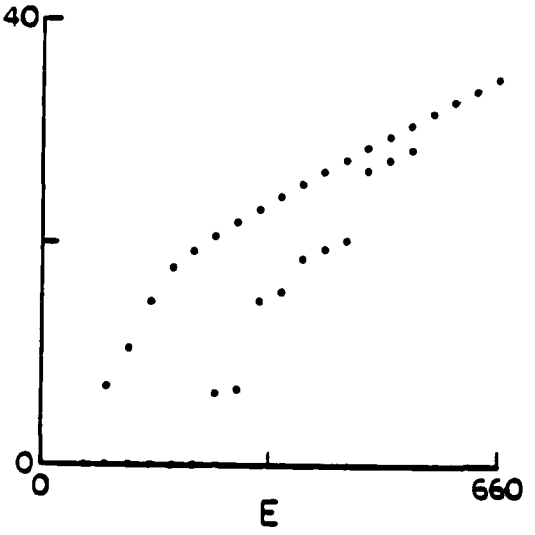

Figure 12.--Continued

(e) Fresnel number=20.

cavity, where the output has been integrated over the transverse direction. As can be seen, all of the outputs exhibit bistability to varying degrees. The smaller effective Fresnel number cases show larger loops and abrupt switching between neighboring input intensity increments while the larger effective Fresnel number cases show smaller loops and more gradual switching. Note the jumbled plot in Fig. 12d for the F_{eff}=2 case. The reason this plot is so jumbled is that for this particular case, the calculations were truncated before the cavity had reached steady state. The convergence to the steady state was much, much slower than in any of the other cases. Indeed, the steady state may never be reached at all. This case will be discussed more later.

Figures 13-16 show the output at various transverse coordinates for the different effective Fresnel numbers. As can be seen, for small effective Fresnel numbers (.002 and .02), the device turns on (i.e., exhibits bistability) in the transverse direction beyond points where the input has fallen to less than 1% of its peak value. Diffraction is strong enough to couple the device together so that it responds as a unit. This coupled response can also be seen in the fact that all points in the transverse direction switch on and off at the same increment in input intensity. Because the entire device switches on at the same time, the integrated curve shows sharp switching.

As one moves to large effective Fresnel numbers (20), the results change. The device no longer switches completely, but rather only part of the device exhibits bistability while the remainder of the device remains low transmitting. The large effective Fresnel number reduces

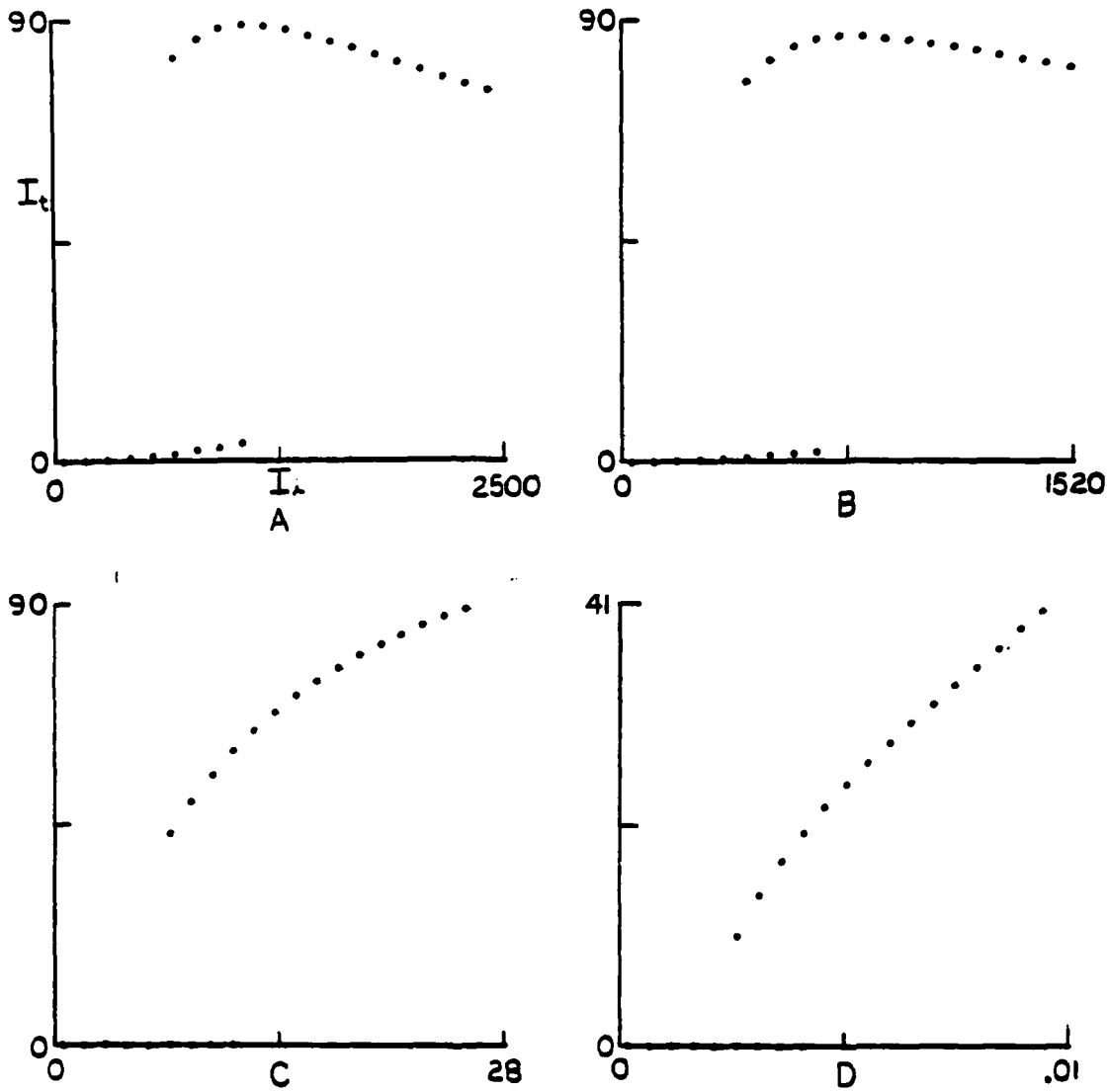

Figure 13. Plots of the output intensity as a function of the input intensity at various transverse points for Fresnel number= .002.

The half maximum of the input occurs at about step 7.
(a) On-axis point.
(b) 5 steps off.
(c) 15 steps off.
(d) 20 steps off.

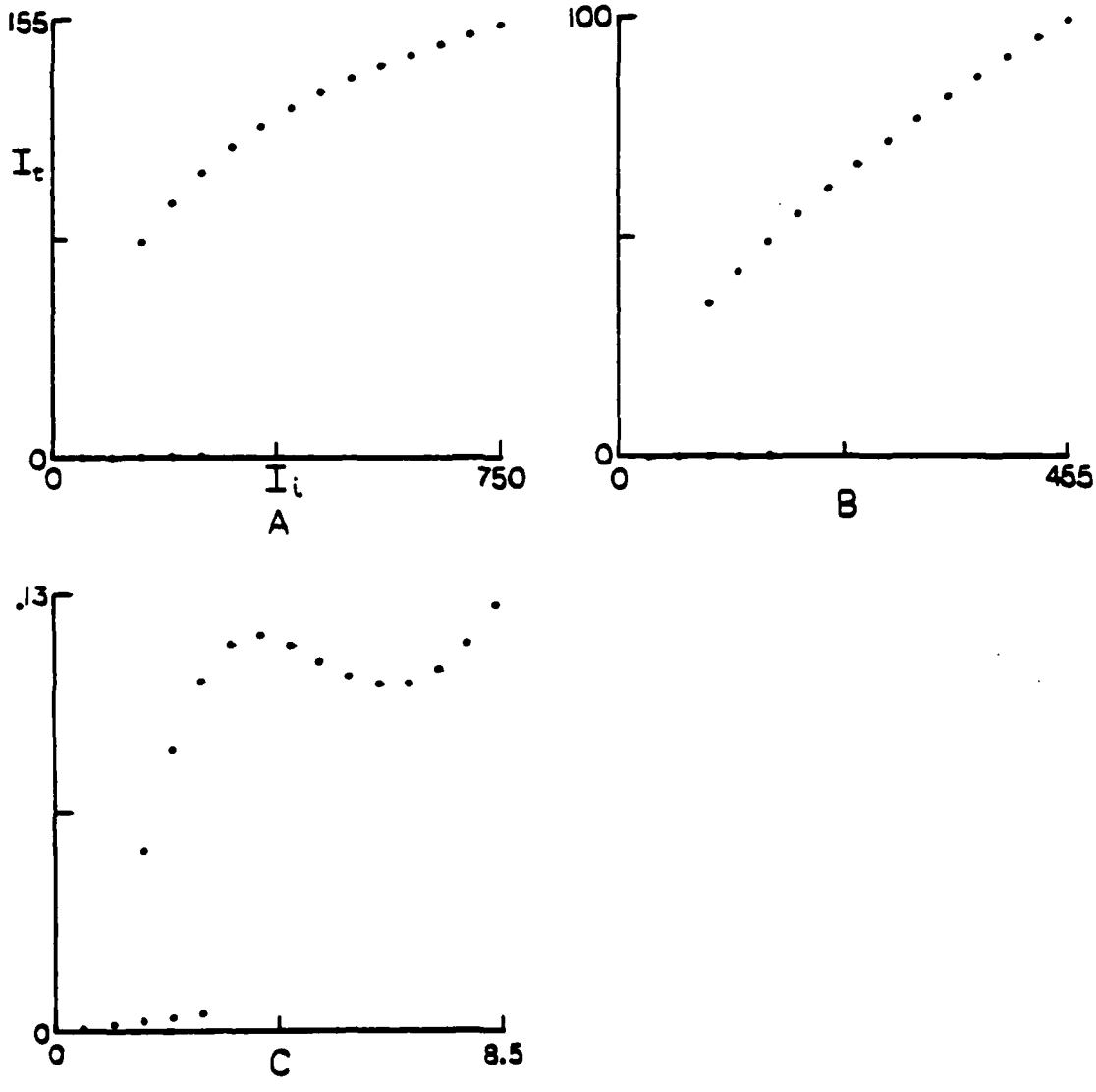

Figure 14. Plots of the output intensity as a function of the input intensity at various transverse points for Fresnel number=.02.

(a) On-axis point.
(b) 5 steps off.
(c) 15 steps off.

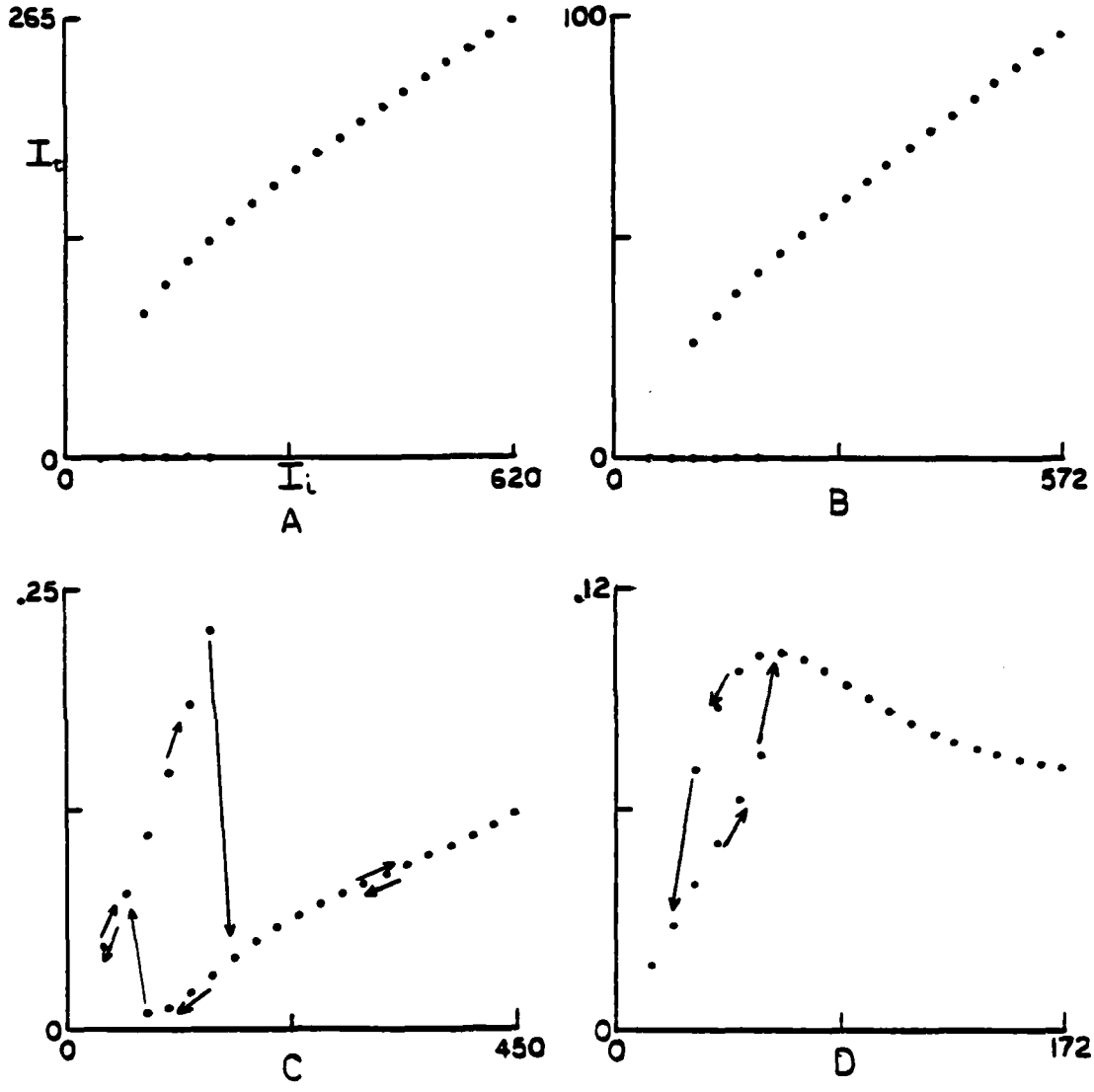

Figure 15. Plots of the output intensity as a function of the input intensity at various transverse points for Fresnel number=.2.

The arrows in (c) and (d) show the directions of the bistable traces. Note the inverted switching in (c) due to self-focusing.

(a) On-axis point.
(b) 2 steps off.
(c) 4 steps off.
(d) 8 steps off.

diffraction so that the cavity no longer responds as a unit. Note that diffraction is so weak that the cutoff between the "on" ring and the "off" ring is very sharp. Also note that the parts of the device which switch on do not do so at the same increment in input intensity. This leads to the slow on and off switching present in the integrated plot.

There is another effect occurring in these calculations, and that is self-focusing. In the small effective Fresnel number limit, diffraction is large enough to overcome the effect of self-focusing, and the output beam is wider than the input beam. At the high effective Fresnel number limit, self-focus ng effects are very small. This was determined by reversing the sign of the cavity and atomic detunings from the laser (which then should lead to self-defocusing) and noting that the beam did not change any in shape. This indicated that focusing/defocusing did not affect the beam profile. In cases between the effective Fresnel number limits, self-focusing did have a noticeable effect. In the case of F_{eff}=.2, self-focusing caused the inverted switching seen in Fig. 15c. As the device switched on, the intracavity intensity was large enough for self-focusing to occur, which drew energy into the center of the beam, thereby decreasing the intensity of the neighboring points. When the signs of the detunings were reversed as discussed above, the beam became shorter and broader, and the inverted switching disappeared and was replaced by normal switching out past the 1%-of-maximum-input point. For the F_{eff}=2 case, the self-focusing conditions produced the jumbled output discussed earlier. When the transverse profile was investigated, it was seen that the device would switch on

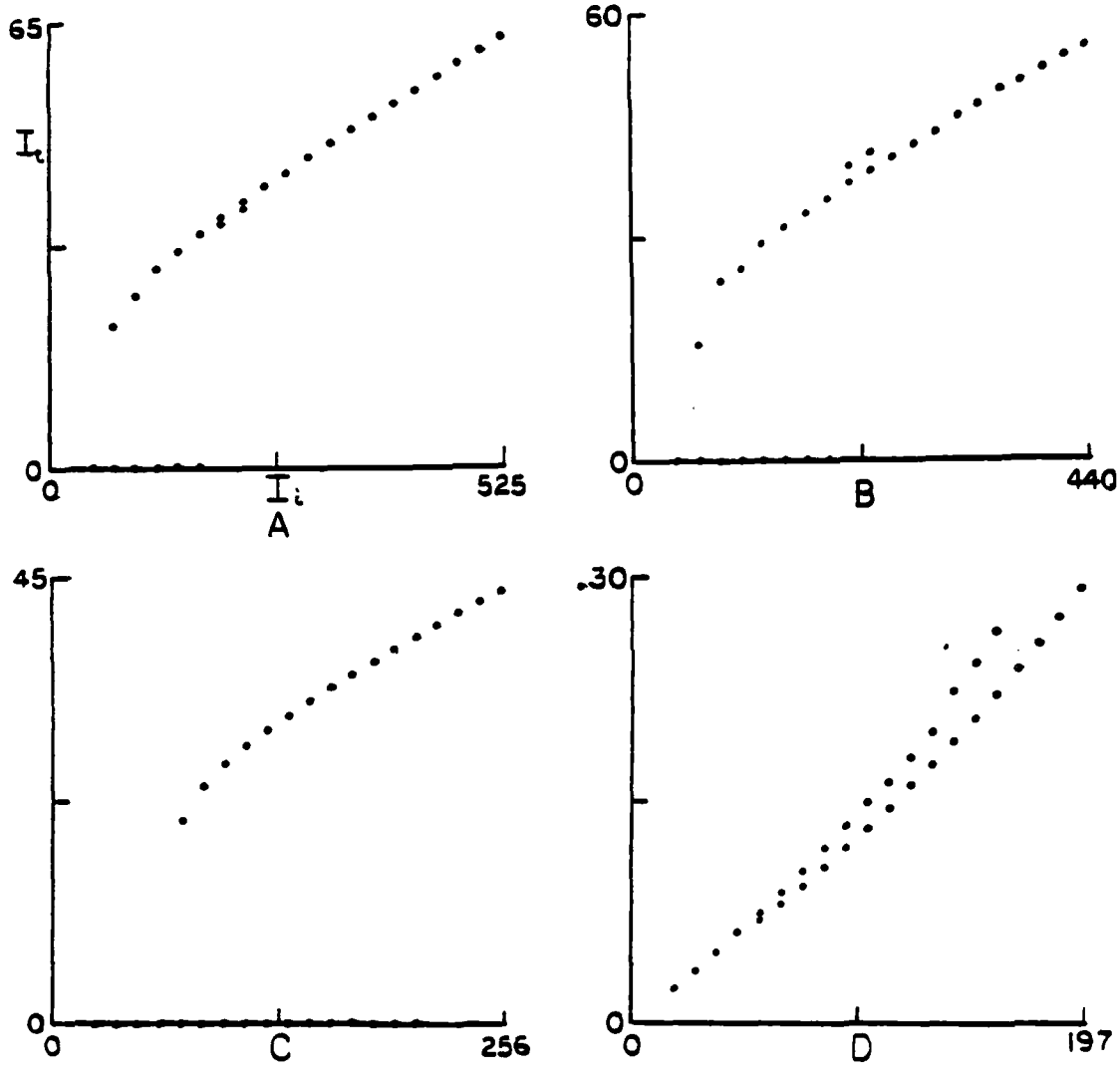

Figure 16. Plots of the output intensity as a function of the input intensity at various transverse points for Fresnel number=20.

(a) On-axis point.
(b) 3 steps off.
(c) 6 steps off.
(d) 7 steps off. Note that the device is no longer bistable at step 7.

partially, much as in the F_{eff}=20 case. However, the high intensity portion of the output profile was not smooth, but had large oscillations in it. These oscillations did not reach a steady state, but rather traded energy between them, one peak growing while the other died down, then vice-versa. It was because of these transient oscillations that the output of the calculations did not reach steady state. When the signs of the detunings were reversed, leading to defocusing, the effects disappeared, and a broader, shorter profile with no oscillations was seen. The device then exhibited normal bistability down to about 5% of peak input, and the rest of the device was not bistable.

A final point can be seen from the figures. As the effective Fresnel number was increased, the intensity required for switch up, as determined from the integrated plots, was reduced. However, the quality of the bistable loop was also affected.

Conclusions

The simulations have shown an interesting dependence of bistability on Fresnel number. The value of $F_{eff} \approx 1$ seems best for complete beam switching and high transmission. If the effective Fresnel number is too large, the device as a whole exhibits poor bistable loops. For small effective Fresnel number, the device shows good bistable loops. However, neighboring bistable devices in integrated optics would have to be separated by many diameters to prevent overlapping due to diffraction. The effect of self-defocusing is to couple the device together more strongly, except at high effective Fresnel numbers. Therefore,

self-defocusing is preferable over self-focusing in causing the device to respond as a unit.

CHAPTER 4

EXPERIMENT IN OPTICAL BISTABILITY

Description of the Experiment

The purpose of the experiment was to investigate how far in the transverse direction an optically bistable device switches on. Due to a variety of reasons, the parameters of the experiment were not those investigated in the theory. This was thought not to be extremely detrimental, however, since it seemed reasonable that the device would switch on or off in essentially the same manner regardless of the specifics of the device. The primary difference between the simulations and the experiment is that the two operate in different limits of the theory. The simulations, as noted earlier, adiabatically eliminated the atomic medium under the concept that the medium was fast with respect to the field. The device used in the experiment, however, functioned in the other limit. Here, the field was fast with respect to the material parameters, and therefore the field followed the material parameters.

The device used in the experiment was made from GaAs and coated with 90% (approximately) reflectivity dielectric coatings (see Fig. 17). The device was approximately 5μ in length. It was supported by a substrate also made of GaAs. A hole was etched in the substrate about 1mm in diameter to allow optical input. The hole size was much bigger than the spot size of the input beam, which was about 10μ. These dimensions,

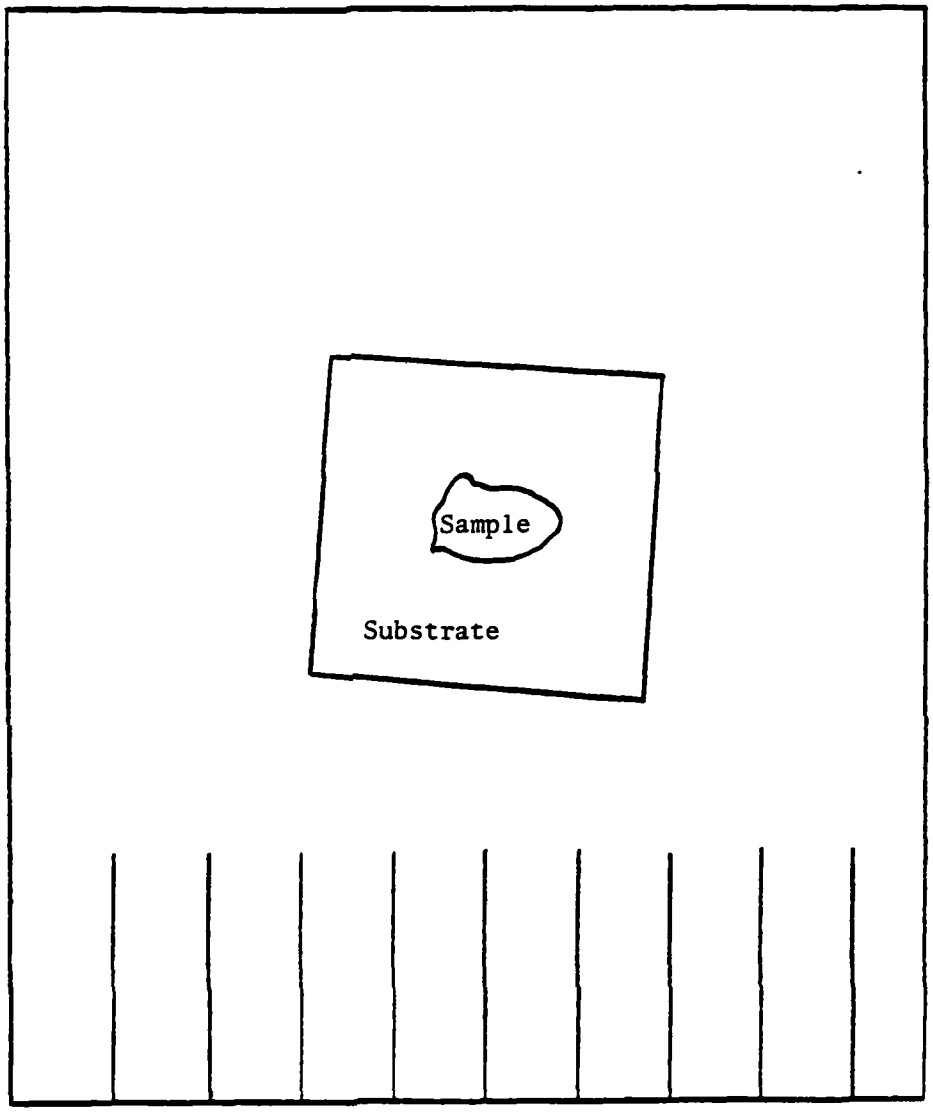

Figure 17. Sketch of sample used in bistability experiment. The ruling at the bottom is a millimeter scale.

combined with a measured finesse of about 8, gave an effective Fresnel number (as defined in Chapter 3) of about 3.

The bistability mechanism in GaAs depends upon the exciton characteristics of the material. The excitons are created by absorption of light quanta and contribute to the absorptive and refractive properties of the material. The exciton absorption can be saturated because as more excitons are created, the orbits begin to overlap thereby shielding the Coulomb attraction between the electron-hole pair, destroying the exciton. As the exciton absorption saturates, the contribution to the refractive index changes. Hence a GaAs cavity changes its transmission peak as the excitonic contribution saturates, giving rise to dispersive bistability as discussed in Chapter 3.

The experimental set-up used is shown in Fig. 18. The Krypton laser was used as the pumping source for the dye laser, which used oxazine 750 perchlorate as the lasing material. The dye laser was useful because it could be tuned, which was a necessity with the bistable device used. The surface roughness of the device reduced the finesse from a theoretical value of 30 to about 16, and background absorption further reduced it to about 8.

The output of the dye laser is continuous wave. As a result it was necessary to insert an acousto-optic modulator to form a pulse that traces out the bistability hysteresis loop. A diode detector monitored the input pulse. A beam expander and lens permitted tight focusing on to the sample. The sample was held in a vacuum within a dewar filled with liquid nitrogen (77°K). Cooling the sample was necessary to observe

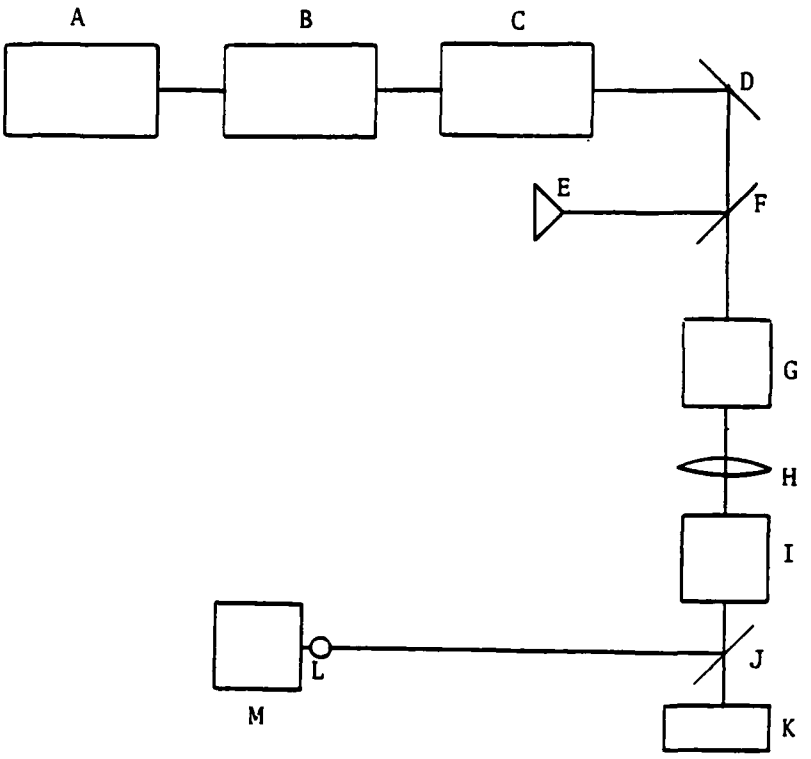

Figure 18. Experimental set-up.

A. Krypton Pump Laser
B. Dye Laser
C. Acousto-Optic Modulator
D. Folding Mirror
E. Diode Detector
F. Beam Splitter
G. Beam Expander
H. Lens
I. GaAs Sample
J. Beam Splitter
K. Photomultiplier Tube Detector
L. Small Aperture on X-Y-Z Translation Stage
M. Photomultiplier Tube Detector

the exciton characteristics of the medium. On the output side of the sample, a lens was used to focus the output onto a small aperture in front of a two inch diameter photomultiplier tube (8852). The beam splitter allowed part of the sample output to go to a large aperture detector to integrate the output over the transverse dimension. The rest of the output from the sample was monitored through the small aperture mounted on an x-y-z translation stage. The aperture used was 15μ in diameter. This size was found to be about 1/5 the full-width at half maximum of the image of the output beam at the aperture. (The beam was magnified 7x.) Hence, the aperture was small compared with the size of the beam at the aperture.

After the apparatus was aligned and the sample output focused on the small-aperture detector, the aperture was centered on the peak of the sample output. Neutral density filters were placed in the beam as needed to prevent the detector from saturating. A photograph of the oscilloscope display of the output pulse viewed through the small detector was taken, and the location of the detector aperture was recorded. Then the aperture was translated in a transverse direction, the output pulse was photographed again, and the location of the aperture was recorded. This procedure was repeated until the input had fallen off to less than 2% of its peak value. The center of the pulse was again found and measured to ensure that it had not changed radically. The aperture was then translated along the same direction but in the opposite sense to the original translation, and the series of photographs was repeated. The process was then repeated for a direction perpendicular to the original direction.

Results

The results of the measurements are shown in Fig. 19 and in Figs. 20-23. Figure 19 shows the input and output profile as measured at the small aperture detector. The input profile was measured by decreasing the intensity of the input below the switch-on level of the device so that no bistability effects could be seen. The plots in Fig. 19 show the input peak normalized to the peak of the output. Note the secondary peaks located on either side of the main peak on both the input and output. No spatial filtering was done to remove them since they were small compared to the peak values.

Figures 20-23 show the output pulse and bistability loop at various transverse points. From these figures, it can be seen that when switch-up occurs, it occurs at least out to a radius where the input has fallen to 2% of its peak value. Also, it appears that the entire device switches at the same input intensity. This would suggest that diffraction, which couples the transverse parts of the beam, is strong enough that the entire device acts as a unit. These results are qualitatively similar to the results obtained from the simulations in Chapter 3 for an effective Fresnel number of a similar order in the defocusing condition.

Note in Figs. 20c and 22c that the transverse locations near the secondary peaks show inverted switching; the simulations also show inverted switching in the focusing case. The cause for inverted switching is the same as in the simulations, i.e., self-focusing or self-defocusing. In the GaAs sample, the refractive index decreases with increased intensity for laser frequencies less than the exciton resonance as is used

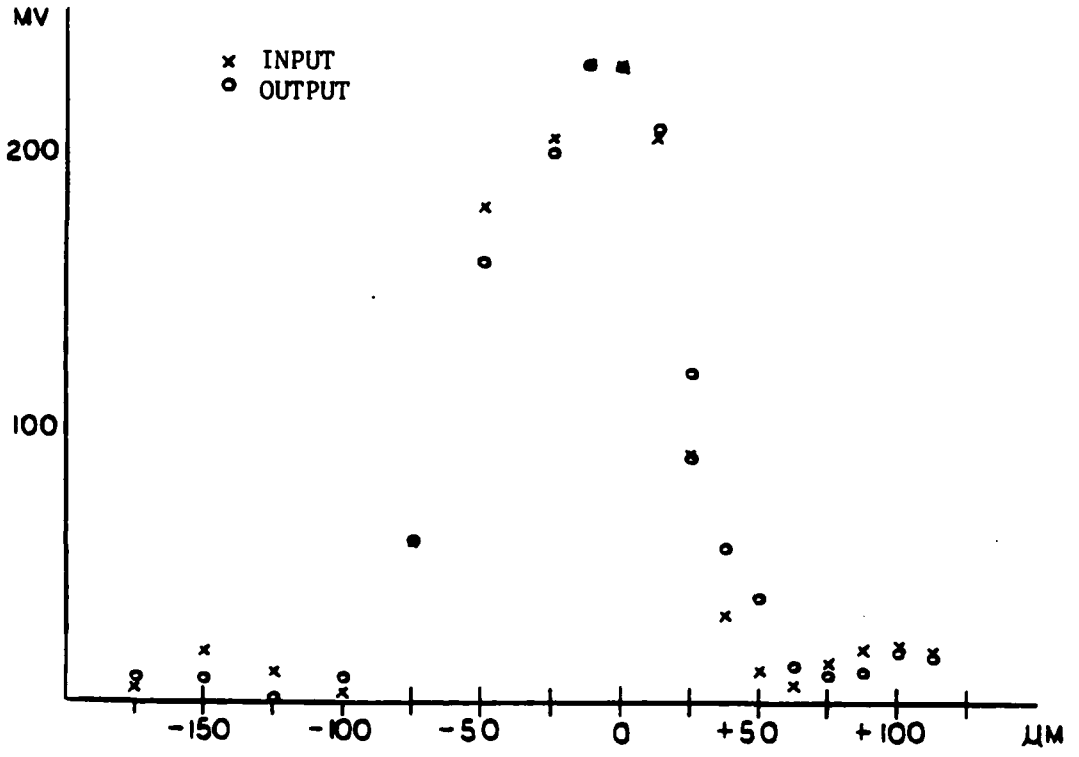

Figure 19. Input and output profiles of the bistable device.

The input was scaled to the peak of the output. The ordinate is the oscilloscope output in units of millivolts. The abscissa shows the location of the aperture in the transverse dimension with respect to output beam center. The units are micrometers.

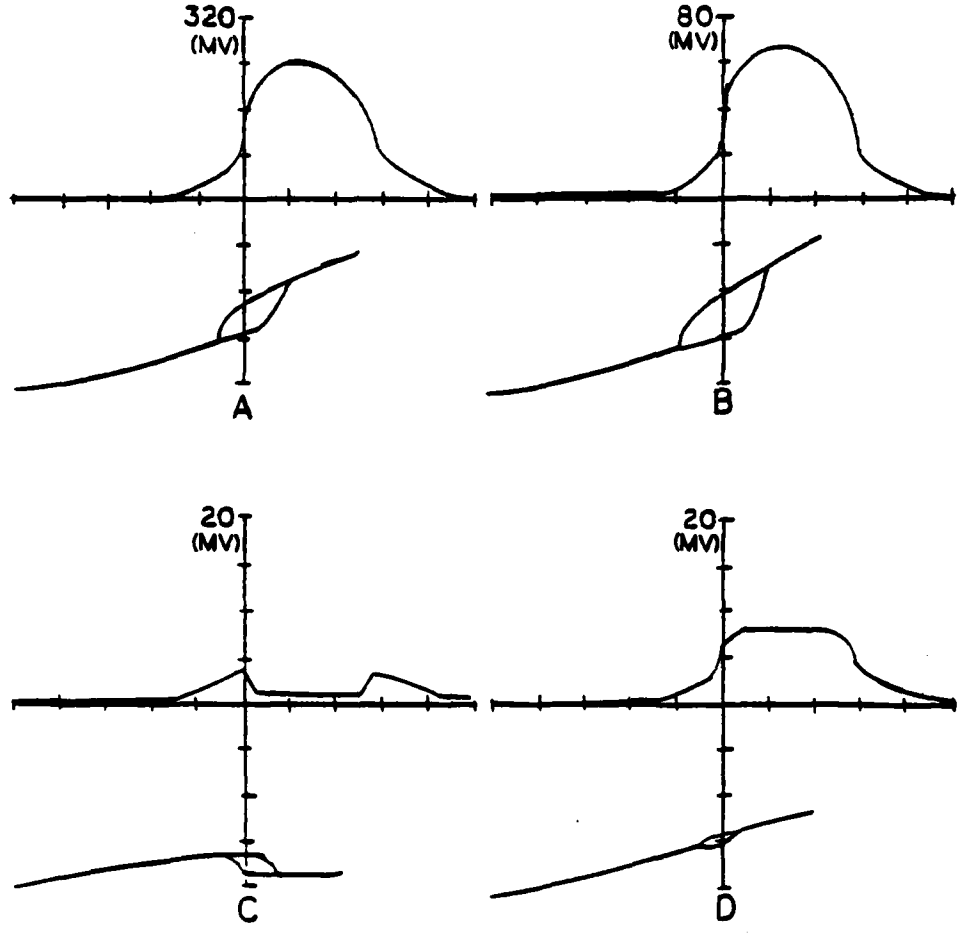

Figure 20. Output of the bistable device at various transverse locations.

The upper curves show the time trace of the output, and the lower curves show the familiar bistable loop for the same output.

(a) On-axis point.
(b) 50μ off axis.
(c) 100μ off axis.
(d) 150μ off axis.

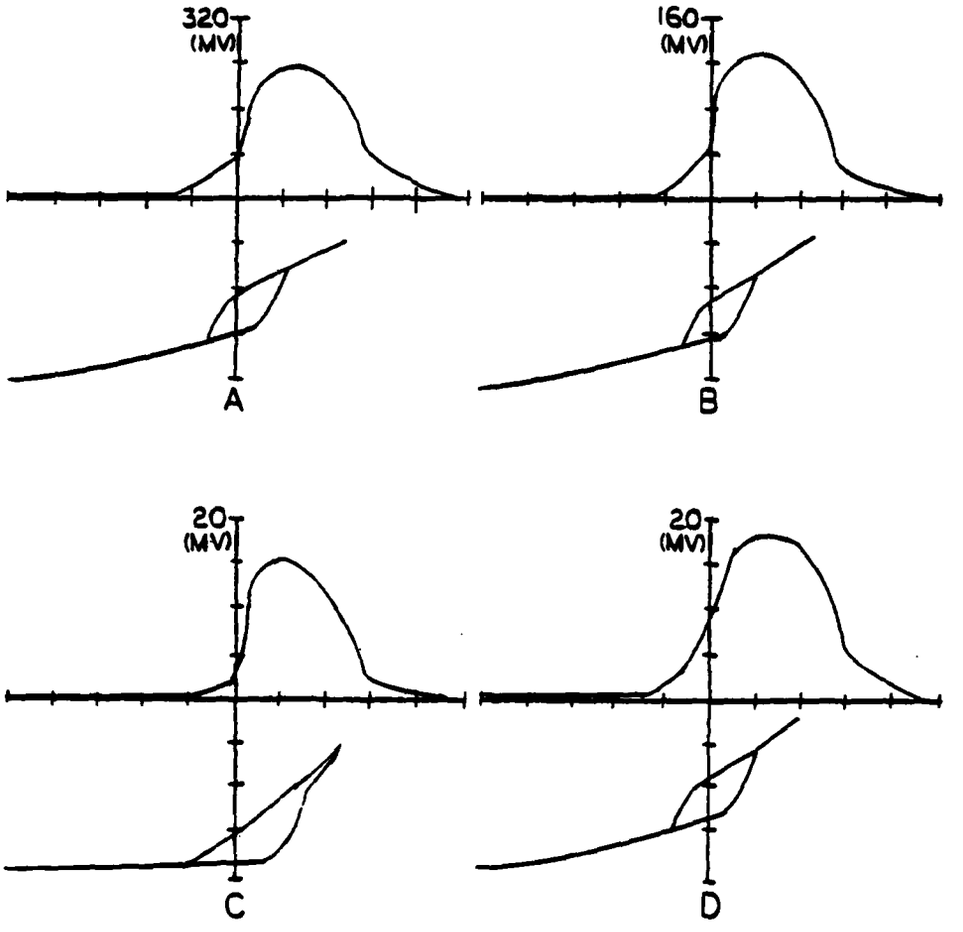

Figure 21. Output of device at various transverse locations, same direction as in Figure 20, but opposite sense.

(a) On-axis point.
(b) 25μ off axis.
(c) 63μ off axis.
(d) 113μ off axis.

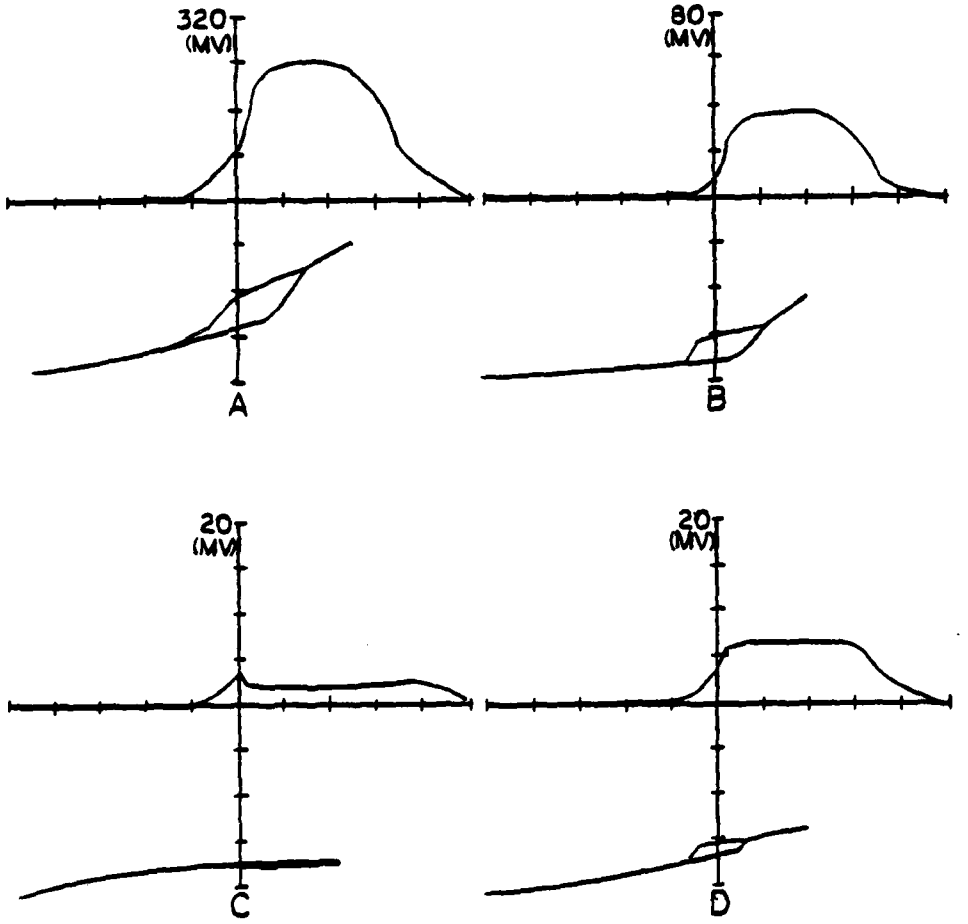

Figure 22. Output of device at various transverse points.

The direction is perpendicular to that shown in Figure 20.

(a) On-axis point.
(b) 50μ off axis.
(c) 100μ off axis.
(d) 125μ off axis.

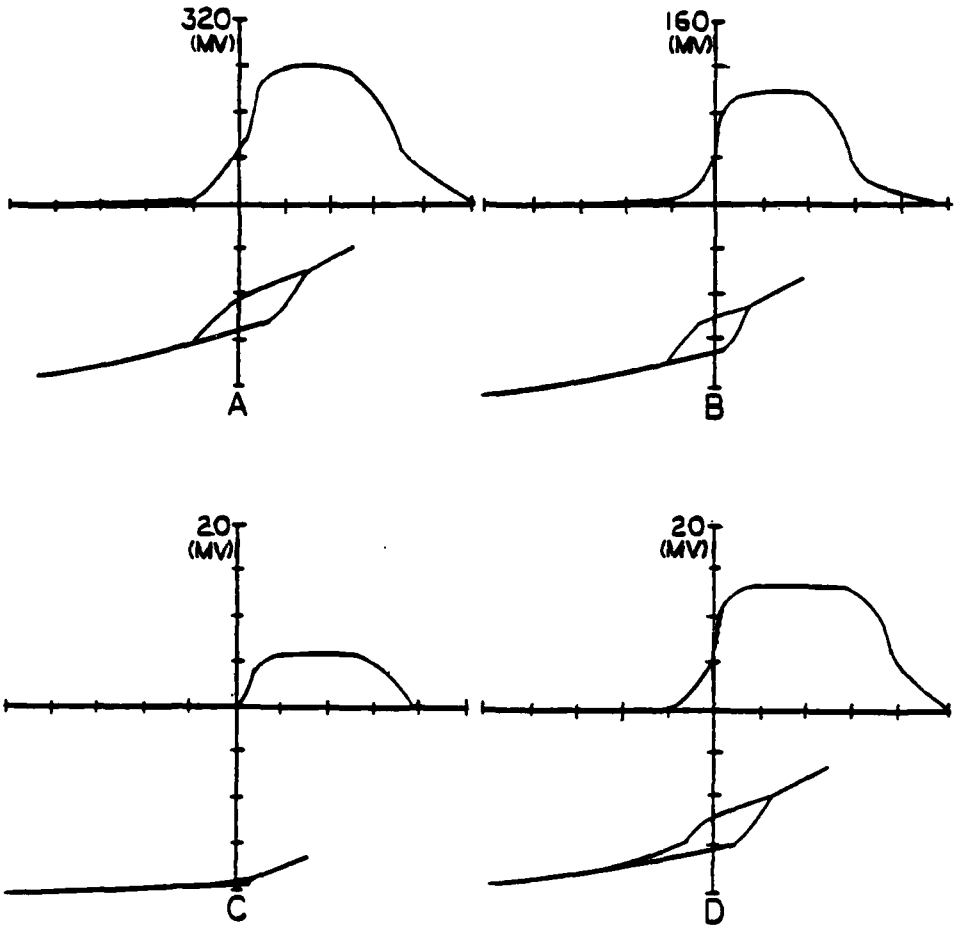

Figure 23. Output of device at various transverse points, same direction as in Figure 22, but opposite sense.

(a) On-axis point.
(b) 50μ off axis.
(c) 88μ off axis.
(d) 150μ off axis.

for bistability. Therefore, self-defocusing occurs. Self-defocusing moves the secondary peaks away from pulse center. The result is to reduce the output suddenly when the device suddenly switches on and there is enough intracavity intensity for self-defocusing to occur.

Conclusions

The results of the first transverse optical bistability experiment indicate that a device with an effective Fresnel number on the order of one switches on as a unit. The results agree with the simulations discussed for the case of $F_{eff} \approx 1$ with self-defocusing.

SELECTED BIBLIOGRAPHY

Agrawal, G. P. and M. Lax, J. Opt. Soc. Am. 69, 1717 (1979).

Allen, L. and J. H. Eberly, Optical Resonance and Two-Level Atoms, John Wiley, New York (1975).

Belic, M., Ph. D. dissertation, Physics Dept., The City College of the City University of New York, New York, NY (1979).

Bonifacio, R., M. Gronchi, and L. A. Lugiato, Nuovo Cimento 53b, 311 (1979).

Bonifacio, R. and L. A. Lugiato, Phys. Rev. A 11, 1507 (1975a).

Bonifacio, R. and L. A. Lugiato, Phys. Rev. A 12, 587 (1975b).

Bonifacio, R. and L. A. Lugiato, Optics Commun. 19, 172 (1976).

Bonifacio, R. and L. A. Lugiato, Lett. Nuovo Cimento, 21, 517 (1978a).

Bonifacio, R. and L. A. Lugiato, Phys. Rev. A 18, 1129 (1978b).

Bonifacio, R., P. Schwendimann, and F. Haake, Phys. Rev. A 4, 302 and 854 (1971).

Burnham, D. C. and R. R. Chiao, Phys. Rev. 188, 667 (1969).

Degiorgio, V., Opt. Commun. 2, 362 (1971).

Dicke, R. H., Phys. Rev. 93, 99 (1954).

Eberly, J. H. and N. E. Rehler, Phys. Lett. A 29, 142 (1969).

Gibbs, H. M., S. L. McCall, and T. N. C. Venkatesan, Phys. Rev. Lett. 36, 1135 (1976).

Gibbs, H. M., S. L. McCall, and T. N. C. Venkatesan, Optics News 5, 6 (1979).

Gibbs, H. M., S. L. McCall, and T. N. C. Venkatesan, Opt. Eng. 19, 463 (1980).

Gibbs, H. M., T. N. C. Venkatesan, S. L. McCall, A. Passner, A. C. Gossard, and W. Wiegmann, Appl. Phys. Lett. 34, 511 (1979).

Gibbs, H. M., Q. H. F. Vrehen, and H. M. J. Hikspoors, Phys. Rev. Lett. 39, 547 (1977).

Gronchi, M. and L. A. Lugiato, Optics Lett. 5, 108 (1980).

Haake, F., J. Haus, H. King, G. Schroder, and R. Glauber, Phys. Rev. Lett. 45, 558 (1980).

Haake, F., H. King, G. Schroder, J. Haus, R. Glauber, and F. Hopf, Phys. Rev. Lett. 42, 1740 (1979a).

Haake, F., H. King, G. Schroder, J. Haus, and R. Glauber, Phys. Rev. A 20, 2047 (1979b).

Lax, M., W. H. Louisell, and W. B. McKnight, Phys. Rev. A 11, 1365 (1975).

MacGillivray, J. C. and M. S. Feld, Phys. Rev. A 14, 1169 (1976).

MacGillivray, J. C. and M. S. Feld, Phys. Rev. A 23, 1334 (1981).

Mattar, F. P., Polytechnic Institute of New York, Farmingdale, New York, private communication, 1981.

Mattar, F. P., H. M. Gibbs, S. L. McCall, and M. S. Feld, Phys. Rev. Lett. 46, 1123 (1981).

McCall, S. L., Appl. Phys. Lett. 32, 284 (1978).

McCall, S. L., Bell Laboratories, Murray Hill, New Jersey, private communication, 1981.

McCall, S. L. and H. M. Gibbs, J. Opt. Soc. Am. 68, 1378 (1978).

McCall, S. L., H. M. Gibbs, G. G. Churchill, and T. N. C. Venkatesan, Bull. Am. Phys. Soc. 20, 636 (1975).

McCall, S. L. and E. L. Hahn, Phys. Rev. 183, 457 (1969).

Miller, D. A. B., S. D. Smith, and A. Johnston, Appl. Phys. Lett. 35, 658 (1979).

Polder, D., M. F. H. Schuurmans, and Q. H. F. Vrehen, Phys. Rev. 19, 1192 (1979).

Rehler, N. E. and J. H. Eberly, Phys. Rev. A 3, 1735 (1971).

Sargent, Murray III, Marlan O. Scully, and Willis E. Lamb, Jr., Laser Physics, Addison-Wesley, Reading, Massachusetts (1977).

Shank, C. V., E. P. Ippen, and S. L. Shapiro, Picosecond Phenomena, Springer-Verlag, Berlin (1978).

Siegman, A. E., An Introduction to Lasers and Masers, McGraw-Hill, New York (1971).

Skribanowitz, N., I. P. Herman, J. C. MacGillivray, and M. S. Feld, Phys. Rev. Lett. 30, 309 (1973).

Smith, P. W. and W. J. Tomlinson, IEEE Spectrum 18, 26 (1981).

Smith, P. W., E. H. Turner, and P. J. Maloney, IEEE J. Quantum Electron. QE-14, 207 (1978).

Smith, S. D. and D. A. B. Miller, New Scientist, 554 (Feb. 21, 1981).

Venkatesan, T. N. C. and S. L. McCall, Appl. Phys. Lett. 30, 282 (1977).

Vrehen, Q. H. F. and J. J. der Weduwe, Phys. Rev. A (to be published).

Yariv, Amnon, Optical Electronics, Holt, Rinehart, and Winston, New York (1976).

Yariv, Amnon, Quantum Electronics, John Wiley & Sons, New York (1975).


DATE
ILME
8